Cell Reports

Article

Bach2 antagonizes leukotriene B4-Ltb4r1-JunB signaling to constrain Tfh13 cell differentiation

Graphical abstract

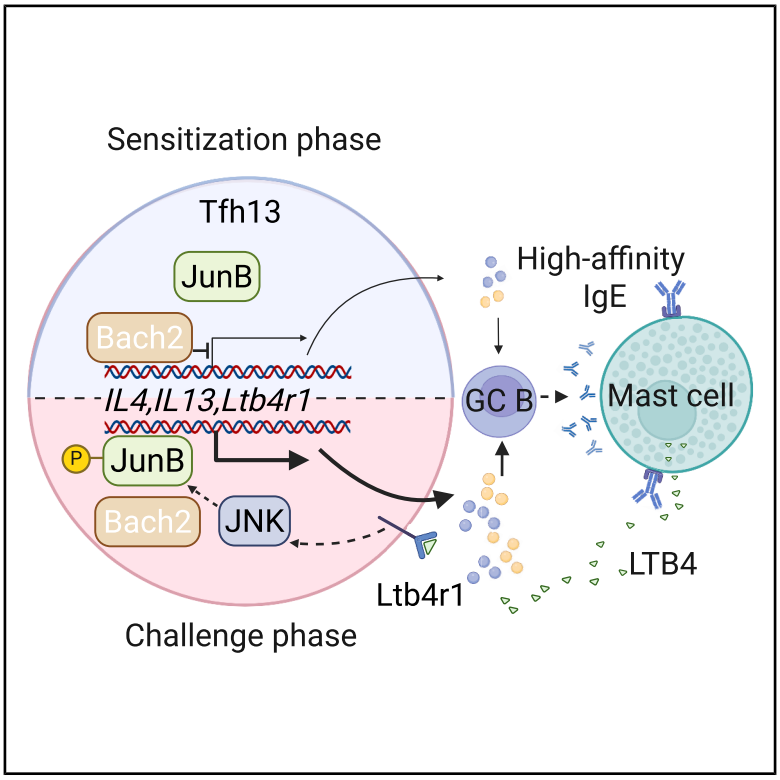

Authors

Lin Zhu, Heng Zhang, Qianwen Hu, Min Zhang, Wenqian Zhang, Chuanxin Huang

Correspondence

dzzhangwenqian@126.com (W.Z.), huangcx@shsmu.edu.cn (C.H.)

In brief

The molecular circuit governing Tfh13 cell development remains poorly understood. Zhu et al. report that the transcription regulator Bach2 plays an opposing role to the LTB4-BLT1-JunB axis in regulating Tfh13 cell development. Mechanistically, Bach2 antagonizes JunB activity by competing for the AP-1 motif at type 2 cytokine loci.

Highlights

- Bach2 suppresses Tfh13 cell development and IgE responses
- The LTB4-BLT1-JunB axis promotes Tfh13 cell development
- Bach2 antagonizes JunB activity by competing for AP-1 motifs at type 2 cytokine loci

Zhu et al., 2026, Cell Reports *45*, 117220
April 28, 2026
https://doi.org/10.1016/j.celrep.2026.117220

CellPress

Cell Reports

CellPress
OPEN ACCESS

Article

Bach2 antagonizes leukotriene B4-Ltb4r1-JunB signaling to constrain Tfh13 cell differentiation

Lin Zhu,[1,2,6] Heng Zhang,[3,6] Qianwen Hu,[4] Min Zhang,[5] Wenqian Zhang,[1,2,*] and Chuanxin Huang[1,2,7,*]

[1]Center for Immune-Related Diseases at Shanghai Institute of Immunology, Ruijin Hospital, Shanghai Jiao Tong University School of Medicine, Shanghai, China

[2]Key Laboratory of Cell Differentiation and Apoptosis of the Chinese Ministry of Education, Shanghai Jiao Tong University School of Medicine, Shanghai, China

[3]Department of Clinical Laboratory, Fudan University Shanghai Cancer Center, Shanghai, China

[4]Clinical Laboratory, Sir Run Run Shaw Hospital, Zhejiang University School of Medicine, Hangzhou, Zhejiang, China

[5]Department of Respiratory and Critical Care Medicine, Shanghai General Hospital, Shanghai Jiao Tong University School of Medicine, Shanghai, China

[6]These authors contributed equally

[7]Lead contact

*Correspondence: dzzhangwenqian@126.com (W.Z.), huangcx@shsmu.edu.cn (C.H.)

https://doi.org/10.1016/j.celrep.2026.117220

SUMMARY

Follicular helper T (Tfh) 13 cells, a rare Tfh subpopulation co-expressing interleukin-4 (IL-4) and IL-13, are uniquely induced by type 2 allergens and essential for high-affinity IgE production. However, the regulatory circuits governing their differentiation remain elusive. Here, we report that transcriptional repressor Bach2 ablation in T cells unexpectedly promotes Tfh13 differentiation and elicits high-affinity IgE responses to type 1 immunity. Tfh13 cells exhibit a distinct transcriptional profile, marked by upregulation of leukotriene B4 (LTB4) receptor 1 (Ltb4r1). Bach2 deficiency initiates Tfh13 cell differentiation, driving an early surge of high-affinity IgE. Upon allergen rechallenge, IgE-mediated LTB4 release activates Ltb4r1 signaling to enhance JunB-dependent expression of type 2 cytokines to amplify Tfh13 polarization. Mechanistically, Bach2 directly suppresses Ltb4r1 transcription and antagonizes JunB activity by competing for the activator protein 1 (AP-1) motif at type 2 cytokine loci. Together, our findings establish Bach2 as a negative regulator of Tfh13 development by antagonizing LTB4-Ltb4r1-JunB signaling.

INTRODUCTION

Allergic responses, which evolved as protective mechanisms against parasitic infections, are now implicated in a range of common human diseases, including asthma and anaphylaxis.[1] Antigen-specific IgE, particularly of high affinity, plays a pivotal role in mediating these responses. Upon crosslinking FcεRI on mast cells and basophils, IgE triggers inflammatory and vasoactive mediator release that drives allergic inflammation.[2,3] Traditionally, aberrant IgE production has been attributed to excessive T helper 2 (Th2) cell activities. However, emerging evidence indicates that the induction of IgE relies on follicular helper T (Tfh) cells, a specialized subset of $CD4^+$ T cells that provide B cell help within germinal centers (GCs) rather than on Th2 cells.[4–6]

Tfh cells are a heterogeneous population with distinct phenotypic and functional characteristics. Subsets including interferon-γ-producing Tfh1, interleukin (IL)-4-producing Tfh2, and IL-17-producing Tfh17 cells have been described.[7–10] Although Tfh2 cells are implicated in the induction of low-affinity IgE responses during certain type 2 immune reactions, they appear insufficient to drive the generation of high-affinity IgE.[11] More recently, a distinct subset termed Tfh13 cells was identified in mouse models of allergy and shown to be essential for the production of anaphylactic high-affinity IgE.[12] Tfh13 cells are typically not induced in response to helminths or type 1 immune stimuli.[12] The relevance of Tfh13 cells in IgE-mediated allergic responses is further supported by their increased frequency in the peripheral blood of patients allergic to food or aeroallergens.[12–14] Transcriptionally, Tfh13 cells are distinct from both conventional Tfh and Tfh2 cells. In addition to expressing canonical Tfh cell markers including chemokine receptor CXCR5, programmed cell death protein 1 (PD-1), and lineage-specific transcription factor BCL6, Tfh13 cells are uniquely characterized by co-production of the type 2 cytokines IL-4, IL-5, and IL-13, as well as expression of the Th2-associated transcription factor GATA3.[12,15]

The extrinsic and intrinsic molecular mechanisms governing Tfh13 cell differentiation are beginning to be understood. A recent study identified the activator protein 1 (AP-1) transcription

factor JunB as a critical driver of Tfh13 cell development and stabilization.[16] Notably, Tfh13 cells are rare, suggesting the presence of stringent regulatory mechanisms that constrain their differentiation to prevent excessive production of high-affinity IgE under physiological conditions or type 1 immune context. Here, we sought to identify transcriptional regulators that restrict Tfh13 cell development in the context of allergic airway inflammation. In this search, we focused on the transcriptional repressor Bach2, a susceptibility gene implicated in multiple autoimmune and allergic disorders, including allergic asthma.[17] Bach2 is expressed in $CD4^+$ T cells and plays a critical role in regulating Th cell differentiation, homeostasis, and effector functions.[18] It maintains Th cells in a naive state and promotes the development of regulatory T (Treg) cells.[19–21] Notably, we and others have demonstrated that Bach2 constrains Tfh cell development by suppressing *Cxcr5* and *C-maf* transcription, thereby preventing autoimmunity.[22–24] Additionally, Bach2 inhibits the differentiation of Th2 cells by directly repressing the transcription of *Il4*, *Il5*, and *Il13*.[22,25] T cell-specific *Bach2*-deficient mice spontaneously develop lethal type 2 allergic airway inflammation.[25] Given these findings, we investigated whether Bach2 might play a specific role in constraining Tfh13 cell differentiation, thereby limiting IgE-mediated allergic responses.

RESULTS

Bach2 deficiency induces an aberrant Tfh13 cell response to type 1 immunity

Tfh13 cells are selectively induced by type 2 immune responses, such as those triggered by model allergens, including house dust mites (HDMs) and *Alternaria alternata* extract (Alt).[12,26] By contrast, type 1 immune responses elicited by viral or certain bacterial infections do not typically support Tfh13 cell differentiation. To determine whether Bach2 deficiency promotes Tfh13 cell generation in the context of type 1 immune stimuli, we generated mice with T cell-specific deletion of *Bach2* by crossing $Bach2^{fl/fl}$ mice with *Cd4*-Cre transgenic mice (hereafter referred to as T-$Bach2^{-/-}$). *Cd4*-Cre littermates were used as wild-type (WT) controls. Mice were intranasally (i.n.) sensitized with lipopolysaccharide (LPS) and 4-hydroxy-3-nitrophenylacetyl-conjugated ovalbumin (NP-OVA) on day 0, followed by i.n. challenge with NP-OVA on days 12 and 19 (Figure 1A).[12] We hereafter refer to this type 1 immunization as LPS+OVA. 6- to 8-week-old T-$Bach2^{-/-}$ mice were selected at an age prior to spontaneous accumulation of Tfh cells and onset of airway inflammation to ensure controlled immunological priming.[22,25]

Unimmunized WT and T-$Bach2^{-/-}$ mice (6–8 weeks of age) exhibited very low yet comparable frequencies of total Tfh cells (defined as $CD4^+CD19^-CD44^+CXCR5^+PD\text{-}1^+$) and GC B cells (defined as $CD19^+Fas^+GL7^+$) in the lung-draining mediastinal lymph nodes (medLNs) (Figures S1A and S1B). LPS+OVA immunization induced a robust expansion of both populations, with substantially higher responses observed in T-$Bach2^{-/-}$ mice than in WT controls (Figures 1B and 1C). The $CXCR5^+PD\text{-}1^+$ population in our analysis also exhibited higher expression of BCL6 and ICOS compared with $CXCR5^-PD\text{-}1^-$ cells, consistent with a *bona fide* Tfh cell phenotype (Figure S1C). Total Tfh cells from T-$Bach2^{-/-}$ mice produced higher amounts of IL-13 than their WT counterparts upon *in vitro* stimulation (Figure S1D). Notably, T-$Bach2^{-/-}$ mice developed a prominent $IL\text{-}4^+IL\text{-}13^+$ population within the Tfh compartment (~10%) in the medLNs (Figure 1B), consistent with the emergence of Tfh13 cells. The identity of these Tfh13 cells was further validated by isotype and BCL6 staining (Figures S1E and S1F). As expected, $IL\text{-}4^+IL\text{-}13^+$ cells were virtually absent in both the total Tfh and $CXCR5^-PD\text{-}1^-$ non-Tfh $CD4^+$ T cell compartments of WT mice (<1%), confirming that type 1 immune stimuli typically fail to induce Tfh13 cell differentiation. A modest but significant increase in $IL\text{-}4^+IL\text{-}13^+$ cells was also observed within the non-Tfh compartment (~2%), although to a lesser extent, suggesting that the regulatory role of Bach2 is more pronounced in Tfh cells than in non-Tfh $CD4^+$ T cells.

Given the critical role of Tfh13 cells in the generation of high-affinity IgE, we next quantified the titers of total and high-affinity NP-binding IgE in the serum and bronchoalveolar lavage fluid (BALF) of T-$Bach2^{-/-}$ and WT mice following LPS+OVA immunization. Total NP-binding IgE was detected using the NP26-BSA substrate, while high-affinity NP-binding IgE was detected exclusively on NP4-BSA. $Bach2^{-/-}$ mice exhibited significantly elevated titers of high-affinity NP-specific IgE in both serum and BALF compared to WT controls (Figure 1D). Total NP-specific IgE levels were also markedly increased in the BALF of immunized T-$Bach2^{-/-}$ mice (Figure 1D). The anaphylactic capacity of serum IgE from T-$Bach2^{-/-}$ mice was further validated using a passive cutaneous anaphylaxis assay (Figure S1G). In addition, T-$Bach2^{-/-}$ mice produced significantly higher levels of NP-specific IgG1, but comparable levels of NP-specific IgM and IgG2c, compared with WT controls (Figure S1H). These findings indicate that the increased IgE production in T-$Bach2^{-/-}$ mice reflects a skewing toward type 2 immunity rather than a global enhancement of the GC response. Notably, high-affinity NP-specific IgE was detectable in T-$Bach2^{-/-}$ mice as early as the sensitization phase (Figure 1E), suggesting that Bach2 restrains early Tfh13 cell-driven IgE responses. Moreover, HDM exposure induced higher frequencies of Tfh13 cells in T-$Bach2^{-/-}$ mice than in WT controls (Figure S1I). Collectively, these findings demonstrate that Bach2 in T cells is essential for restraining Tfh13 cell development and the production of high-affinity IgE.

Although previous studies have shown that Bach2 deficiency impairs Treg cell differentiation and reduces the formation of follicular regulatory T (Tfr) cells,[19,27] which are known to modulate Tfh13 cell-driven IgE responses,[28] Treg-specific *Bach2*-deficient mice failed to generate Tfh13 cells or produce high-affinity IgE in response to LPS+OVA immunization (Figure S2). These findings indicate that the enhanced Tfh13 differentiation and IgE response observed in T-$Bach2^{-/-}$ mice is not attributable to defective Tfr cell function in our experimental settings.

To assess whether exaggerated Tfh13 responses and elevated high-affinity IgE production contribute to allergic airway inflammation in T-$Bach2^{-/-}$ mice, we examined lung histopathology following LPS+OVA immunization. H&E staining revealed marked immune cell infiltration in the lung tissues of T-$Bach2^{-/-}$ mice compared to WT mice (Figure 1F). Goblet cell metaplasia and mucus hypersecretion, hallmarks of allergic airway disease, were evaluated by Alcian blue-periodic acid

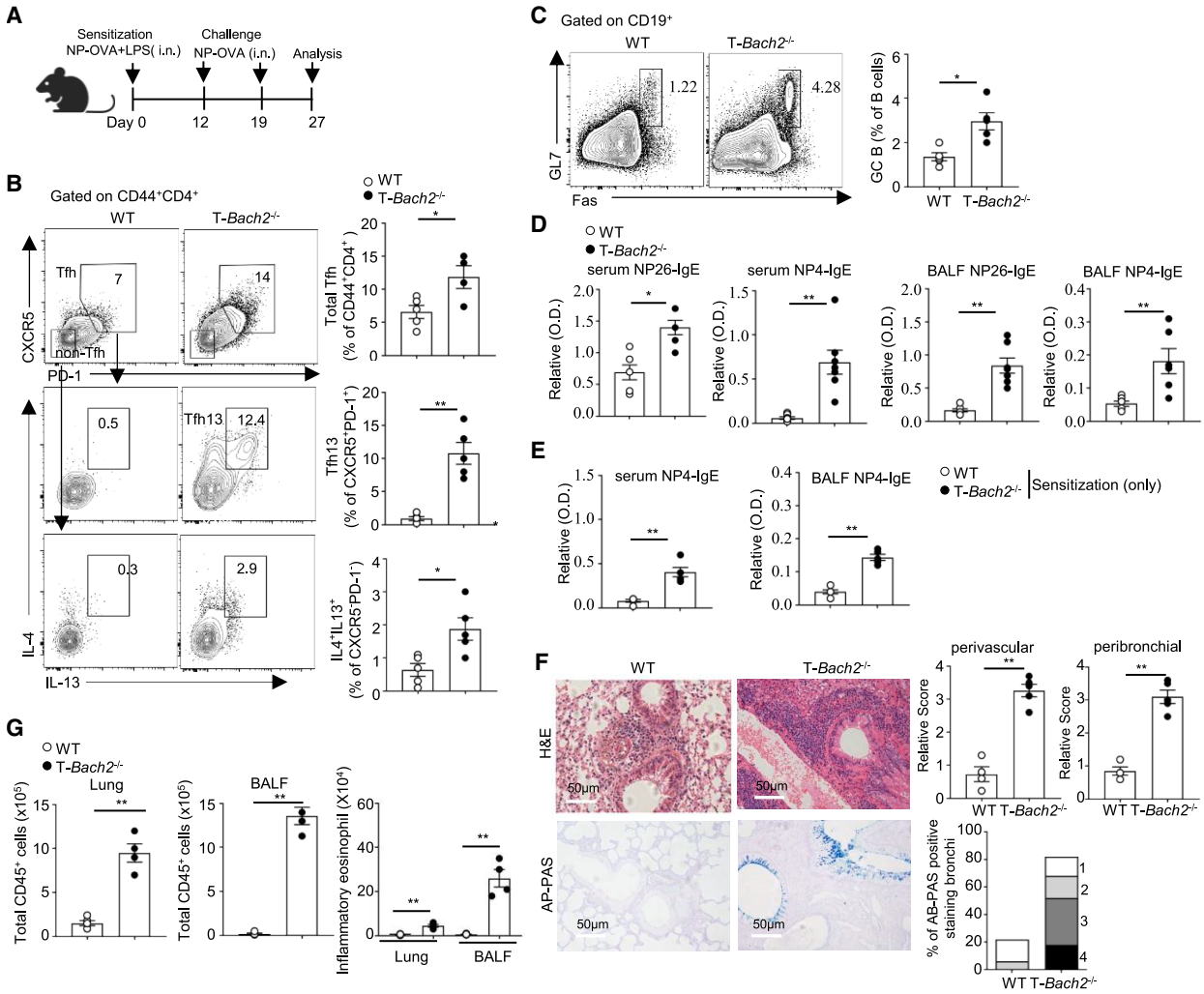

Figure 1. Bach2 deficiency in CD4$^+$ T cells promotes an aberrant Tfh13 cell response to type 1 immunity

(A) Experimental design for LPS+OVA immunization in the induced asthma model. Mice were i.n. treated with 2 μg of LPS and 25 μg of NP16-OVA (sensitization). On days 12 and 19, mice were i.n. challenged with 10 μg of NP16-OVA (challenge) and analyzed on day 27.

(B) Representative flow plots and quantifications showing the frequencies of total CXCR5$^+$PD1$^+$ Tfh cells among CD44$^+$CD4$^+$ T cells, IL-4$^+$IL-13$^+$ Tfh13 among total Tfh cells, and IL-4$^+$IL-13$^+$ cells among non-Tfh cells.

(C) Representative flow plots and quantifications showing the frequencies of Fas$^+$GL7$^+$ GC B cells among CD19$^+$ B cells.

In (B) and (C), the medLNs were collected for analysis.

(D) Relative levels of high-affinity NP4-binding and total NP26-binding IgE in the serum and BALF of mice following LPS+OVA immunization, determined by ELISA. O.D., optical density.

(E) Relative levels of high-affinity NP4-binding IgE in the serum and BALF of mice following sensitization only, determined by ELISA.

(F) Representative H&E and AB-PAS staining of lung sections. Quantifications of perivascular and peribronchial inflammation, as well as goblet cell metaplasia, are shown underneath. Scale bars: 50 μm.

(G) Quantifications of the total number of CD45$^+$ immune cells and inflammatory eosinophils in the lungs and BALF.

Each symbol represents one mouse. Data are presented as means ± SEM and are representative of at least two independent experiments with at least four mice per group. *$p < 0.05$ and **$p < 0.01$ (two-tailed t test). See also Figures S1–S3.

Schiff (AB-PAS) staining. Intense AB-PAS staining was observed in the bronchial epithelium of T-*Bach2* mice, indicating pronounced mucus production, whereas minimal staining was detected in WT lungs (Figure 1F). Flow cytometric analysis further showed elevated numbers of CD45$^+$ immune cells in both the lung and BALF of T-*Bach2*$^{-/-}$ mice (Figure 1G). Notably, inflammatory eosinophil accumulation, a key feature of hyper-IgE phenotypes and allergic asthma, was significantly elevated in both compartments (Figures 1G and S3). These findings demonstrate that Bach2 is required to constrain Tfh13-mediated responses and prevent IgE-driven allergic airway inflammation.

Bach2 restrains spontaneous Tfh13 cell development under steady-state conditions

T-*Bach2*$^{-/-}$ mice spontaneously develop excessive Tfh cell responses in the spleen starting from 3 months of age.[22,25] To

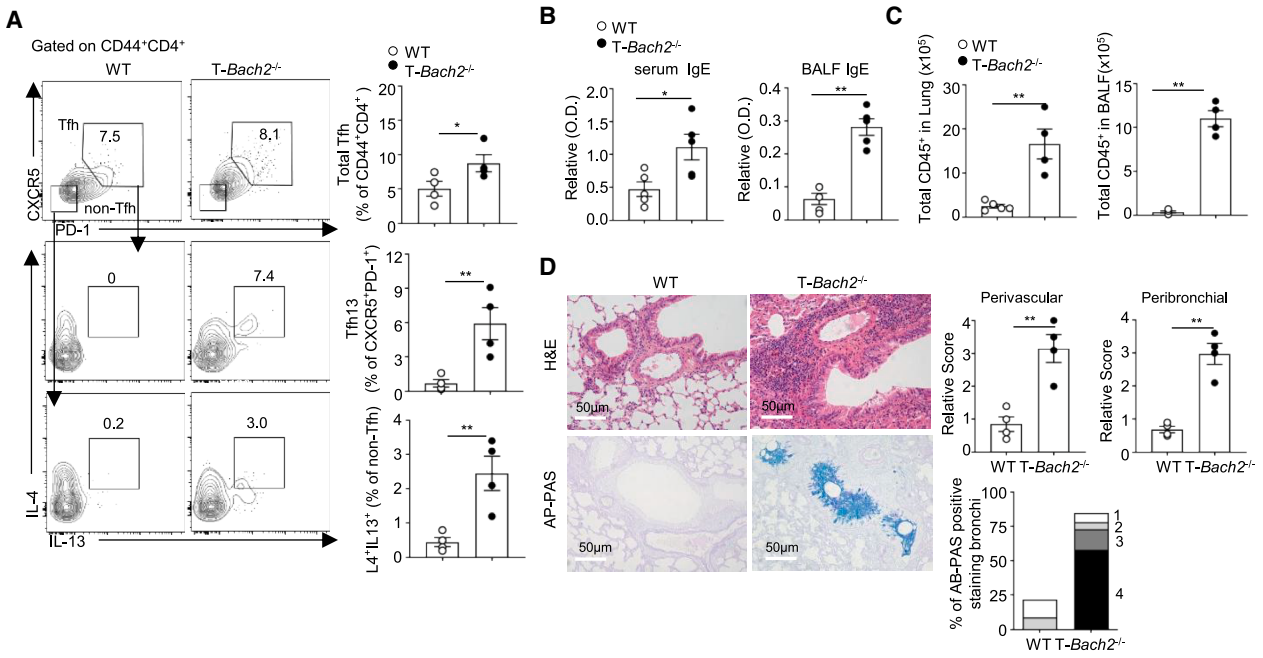

Figure 2. Bach2 restrains spontaneous Tfh13 cell development under steady-state conditions

(A) Representative flow plots and quantifications of the percentages of total Tfh cells among $CD44^+CD4^+$ T cells, IL-4^+Il-13^+ Tfh13 cells among total Tfh cells, and IL-4^+Il-13^+ cells among non-Tfh cells in the medLNs of mice at the age of 6–8 months.

(B) Relative levels of IgE in the serum and BALF, measured by ELSIA. O.D., optical density.

(C) Quantifications of total cell numbers of $CD45^+$ immune cells in the lungs and BALF.

(D) Representative H&E and AB-PAS staining of lung sections and quantifications. Scale bars: 50 μm.

6- to 8-month-old T-*Bach2*$^{-/-}$ and WT mice were subjected to analysis (A–D). Each symbol represents one mouse. Data are presented as means ± SEM and are representative of at least two independent experiments. *$p < 0.05$ and **$p < 0.01$ (two-tailed *t* test). See also Figure S4.

determine whether these mice also spontaneously generate Tfh13 cells when they aged, we analyzed $CD4^+$ T cell populations in 6- to 8-month-old T-*Bach2*$^{-/-}$ mice. Consistent with previous findings,[22] T-*Bach2*$^{-/-}$ mice exhibited significantly higher frequencies of total Tfh cells in the medLNs compared to their WT littermates (Figure 2A). Notably, the frequencies of Tfh13 cells and IL-4/IL-13-co-expressing non-Tfh cells were significantly increased in T-*Bach2*$^{-/-}$ mice compared to WT mice (Figure 2A). ELISA analysis further revealed elevated IgE levels in the serum and BALF of T-*Bach2*$^{-/-}$ mice (Figure 2B). Histological examination demonstrated severe immune cell infiltration and increased mucus production in the lungs of aged T-*Bach2*$^{-/-}$ mice (Figure 2C). Flow cytometric analysis further confirmed a significant increase in $CD45^+$ immune cells and inflammatory eosinophils in both the lung and BALF of T-*Bach2*$^{-/-}$ mice compared to WT mice (Figure 2D). Additionally, we detected a robust Tfh13 population in the spleens of aged T-*Bach2*$^{-/-}$ mice but not WT littermates (Figure S4). These findings collectively demonstrate that Bach2 in T cells is essential for restraining the formation of Tfh13 cells under steady-state conditions.

Tfh13 cells display a distinct transcription program from conventional Tfh cells

Tfh cells constitute a heterogeneous population encompassing distinct subsets at varying developmental stages.[8–10] To investigate the impact of Bach2 deficiency on Tfh heterogeneity, we performed single-cell RNA sequencing (scRNA-seq) on total $CD4^+CD44^+CXCR5^+PD\text{-}1^+$ Tfh cells isolated from the medLNs of 6- to 8-week-old T-*Bach2*$^{-/-}$ and WT mice following LPS+OVA immunization. Unsupervised graph-based clustering of $CD4^+$ T cells revealed six transcriptionally distinct clusters (Figures 3A and 3B). Cluster 1 was identified as Tfr cells, characterized by high expression of *Foxp3*, *Ctla4*, and *Il2ra*. Cluster 2 corresponded to Tfh13 cells, while cluster 3 represented conventional effector Tfh (cTfh) cells, marked by elevated expression of canonical Tfh genes including *Pdcd1*, *Cxcr5*, and *Il21* (Figures 3A and 3B). Tfh13 cells were distinguished by high expression of the type 2 cytokines *Il5* and *Il13*, as well as the transcription factor Gata3. Clusters 4 and 5 were annotated as memory T cell populations, with cluster 4 exhibiting high expression of *Ccr7* and *Sell*, consistent with a central memory phenotype. Cluster 6 comprised proliferating T cells expressing markers of cell cycle progression such as *Mki67* and *Mcm2* (Figures 3A and 3B). T-*Bach2*$^{-/-}$ mice exhibited an increased frequency of cTfh cells and a concomitant reduction in Tfr cells relative to WT controls, consistent with previous reports that Bach2 restrains Tfh cell differentiation while supporting Tfr cell development.[22,23,27,29] Notably, Tfh13 cells were readily detected in T-*Bach2*$^{-/-}$ mice but were virtually absent in WT mice (Figure 3A), underscoring a critical role for Bach2 in suppressing Tfh13 cell emergence.

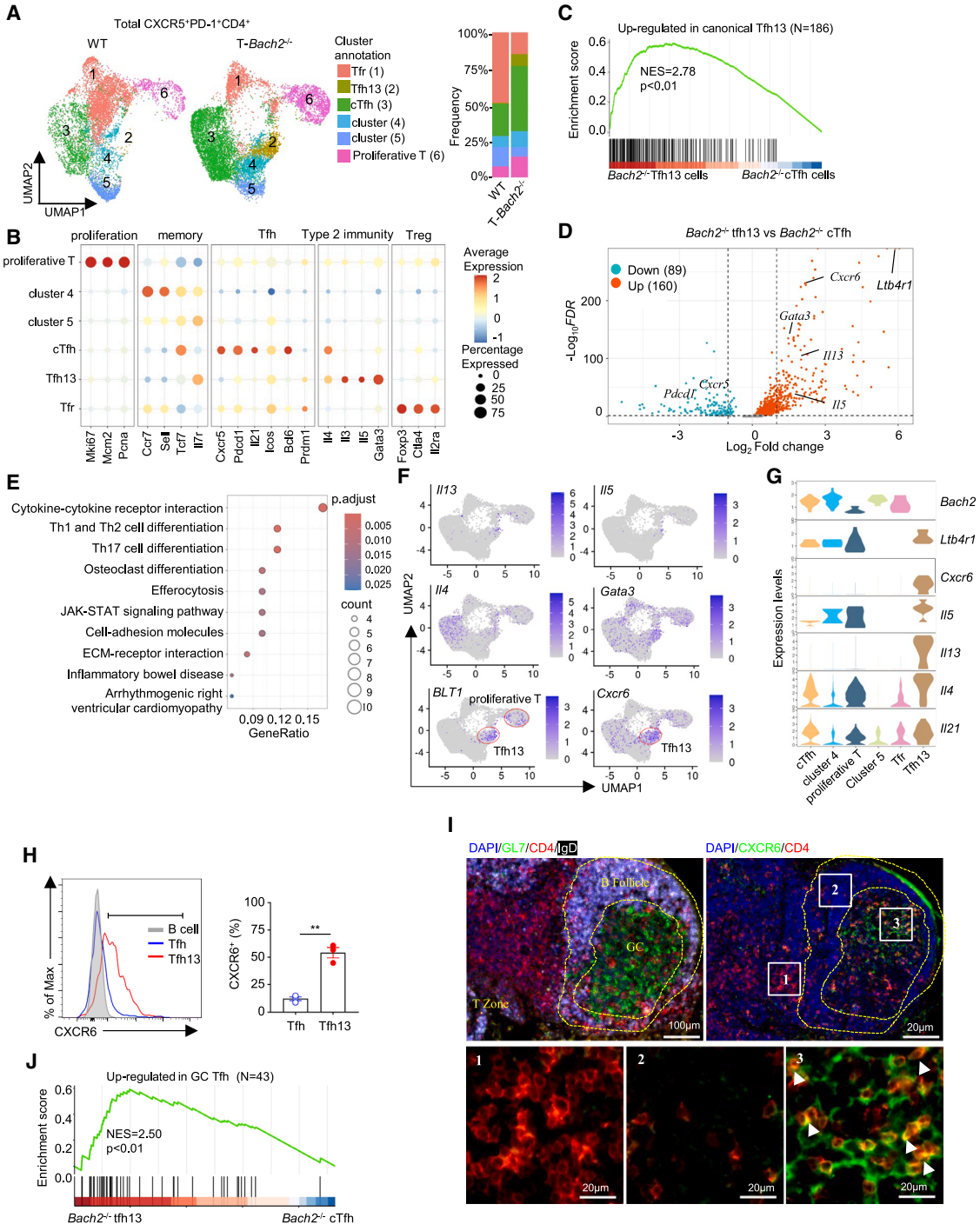

Figure 3. A distinct Tfh13 population is expanded in T-*Bach2*$^{-/-}$ mice

(A) Uniform manifold approximation and projection (UMAP) plot showing six cell clusters of total CXCR5^{+}PD1^{+} Tfh cells isolated from the medLNs of WT and T-*Bach2*$^{-/-}$ mice following LPS+OVA immunization. Proportions of each cluster within the Tfh population are shown (right).

(B) Dot plot showing the relative expression of selected marker genes across various cell clusters.

(C) GSEA of upregulated genes in canonical Tfh13 cells induced by ALT+OVA immunization (GSM3892344) in Tfh13 cells versus Tfh cells in T-*Bach2*$^{-/-}$ mice.

(D) Volcano plot of genes significantly upregulated (red) or downregulated (blue) in Tfh13 cells versus Tfh cells from T-*Bach2*$^{-/-}$ mice. Select genes of interest are labeled.

(E) Gene Ontology categories enriched for significantly upregulated genes in Tfh13 cells versus Tfh cells from T-*Bach2*$^{-/-}$ mice.

(F) Feature plots showing the relative expression of indicated genes across various Tfh clusters from T-*Bach2*$^{-/-}$ mice.

(legend continued on next page)

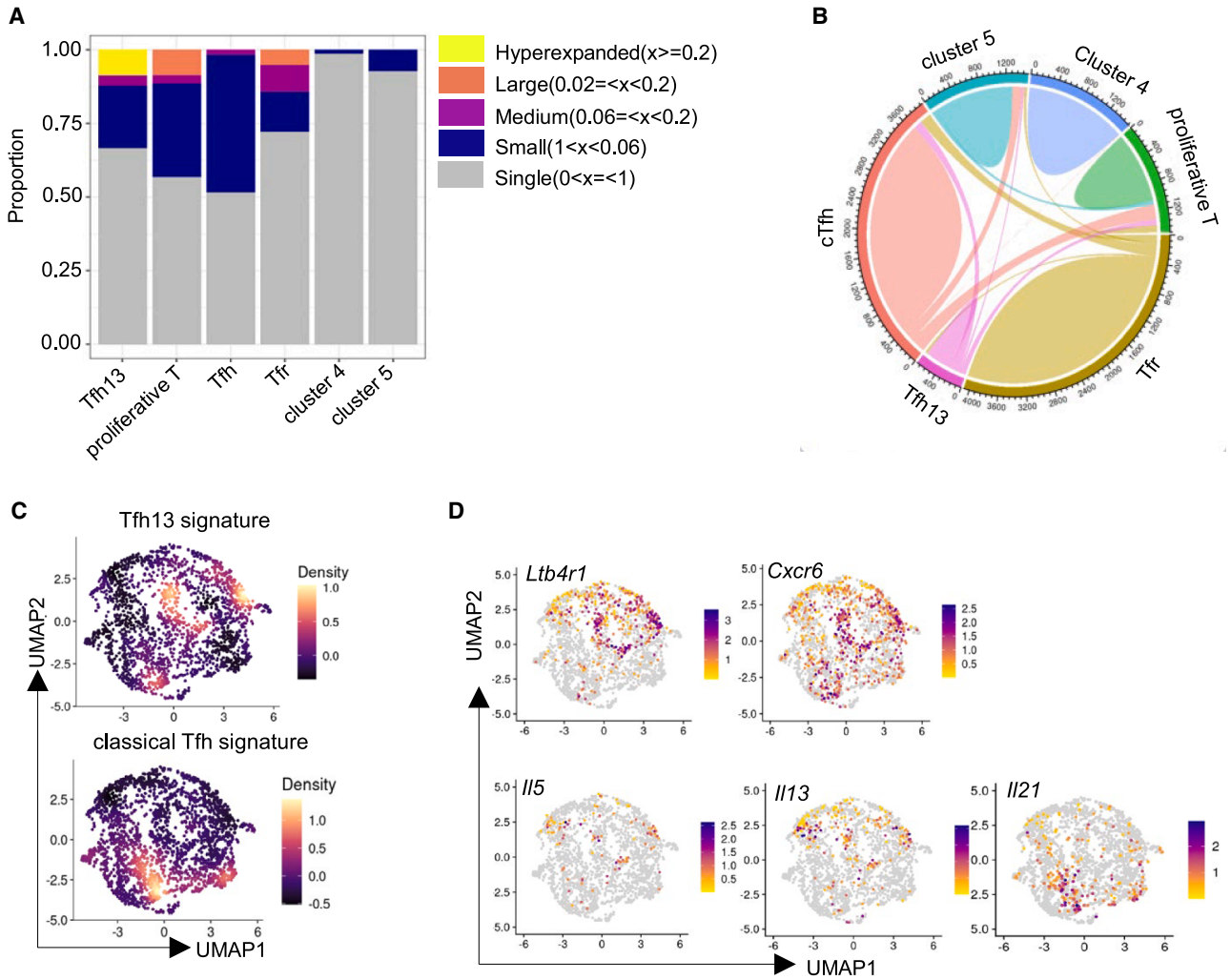

Figure 4. The inferred developmental trajectories of Tfh13 cells

(A) Bar plot showing the distribution of TCR clonotypes by size across cell clusters. X denotes the frequency of each clonotype, defined by its unique paired TCRα and TCRβ sequences.

(B) Chord diagram illustrating TCR clonal overlap among distinct cell subtypes. Links represent shared clonotypes between clusters.

(C) Feature plots showing enrichment of Tfh13- and cTfh-associated transcriptional signatures within the proliferative T cell cluster from T-*Bach2*$^{-/-}$ mice.

(D) Feature plots depicting the expression of indicated genes within the proliferative T cell cluster from T-*Bach2*$^{-/-}$ mice.

To validate the identity of Tfh13 cells induced by LPS+OVA immunization in *T-Bach2*$^{-/-}$ mice, we performed gene set enrichment analysis (GSEA) using a previously defined Tfh13 gene signature derived from WT mice immunized with Alt+OVA.[12] Tfh13 cells from T-*Bach2*$^{-/-}$ mice showed significant enrichment of this canonical Tfh13 transcriptional program (Figure 3C), supporting their phenotypic and functional similarity to *bona fide* Tfh13 cells.

We next sought to delineate the transcriptional signature of Tfh13 cells in T-*Bach2*$^{-/-}$ mice following LPS+OVA. Compared to cTfh cells, Tfh13 cells exhibited 160 upregulated and 89 downregulated genes (false discovery rate [FDR] < 0.05; fold change > 1.5) (Figure 3D). In line with previous findings,[12] Tfh13 cells exhibited increased expression of *Il13* and *Gata3*, alongside reduced levels of *Pdcd1*, *Cxcr5*, and *Il21* (Figure 3D). Pathway enrichment analysis indicated that upregulated genes

(G) Violin plot showing the relative expression levels of selected genes in various Tfh clusters from WT mice immunized with ALT+OVA (GEO: GSE132798).

(H) Flow cytometric analysis of CXCR6 protein expression and quantification in the indicated cell type.

(I) Representative immunofluorescence staining of the medLN section with the indicated antibodies. The dotted yellow line outlines GCs and B follicles. Parts of the stained area were enlarged in the corresponding white rectangle. Nuclei were visualized with DAPI. Arrows indicate CXCR6^{+}CD4^{+} T cells.

(J) GSEA of upregulated genes in GC-resident Tfh cells (GEO: GSE147035) in *Bach2*$^{-/-}$ Tfh13 cells versus *Bach2*$^{-/-}$ Tfh cells.

were associated with cytokine-cytokine receptor interactions and cell adhesion molecules (Figure 3E), suggesting augmented effector potential and altered positioning within the GC niche.

Among the top upregulated genes in Tfh13 cells were *Cxcr6*, encoding the CXC chemokine receptor 6, and *Ltb4r1*, which encodes the high-affinity receptor for leukotriene B4 (LTB4) (Figure 3D). Both genes were uniquely upregulated in Tfh13 cells compared to other Tfh subsets in T-*Bach2*$^{-/-}$ mice, as well as in canonical Tfh13 cells relative to other Tfh subsets from WT mice immunized with ALT+OVA (Figures 3F and 3G).[12] Flow cytometric analysis further validated elevated surface expression of CXCR6 protein in *Bach2*-deficient Tfh13 cells (Figure 3H).

CXCR6, a marker of memory T cells, interacts with its ligand CXCL16 to mediate niche retention and spatial positioning within both lymphoid and non-lymphoid tissues.[30] The CXCR6-CXCL16 axis facilitates T cell access to survival and stimulatory signals by guiding their localization within specialized microenvironments. Previous transcriptomic analyses have indicated high *Cxcr6* expression in GC-resident Tfh cells.[31] Consistent with this, immunofluorescence staining revealed robust CXCR6 protein expression in GC-resident Tfh cells, with minimal expression in non-GC Tfh cells and CD4$^+$ T cells localized to the T cell zone (Figure 3I), supporting its role as a GC-associated marker. Interestingly, we also observed the accumulation of CXCR6$^+$CD4$^-$ structures within the GCs (Figure 3I), which may correspond to CD169$^+$ subcapsular sinus macrophage-derived microvesicles known to traffic into GCs and interact with follicular dendritic cell networks.[32] To determine whether Tfh13 cells preferentially localize to GCs, we performed GSEA using a previously defined GC-resident Tfh signature.[31] Tfh13 cells from T-*Bach2*$^{-/-}$ mice displayed significant enrichment for this signature relative to cTfh cells (Figure 3J), suggesting that Tfh13 cells may be spatially confined to the GC niche, potentially via CXCR6-mediated mechanisms.

The inferred developmental trajectories of Tfh13 cells

Extensive studies have highlighted the considerable plasticity and interconversion among Tfh subsets.[4,10,33,34] To investigate the developmental relationships between Tfh subsets in T-*Bach2*$^{-/-}$ mice, we performed TCR immune profiling. All Tfh clusters, except cluster 4, exhibited clonal expansion, with notable differences in clonal magnitude across subsets (Figure 4A). Among these, Tfh13 cells exhibited the most pronounced clonal expansion. As anticipated, we observed varying degrees of TCR sharing between Tfh subsets (Figure 4B). Importantly, shared TCR clonotypes were detected between Tfh13 cells, cTfh cells, and proliferating T cells (Figure 4B), supporting a model in which these cell types are developmentally interconnected.

It is likely that certain proliferative T cells expand, acquire effector activity, and subsequently differentiate into effector subsets, including Tfh13 and cTfh cells. We hypothesized that precursors committed to the Tfh13 lineage may reside within the proliferative T cell cluster. To test this, we performed sub-clustering analysis of the proliferative T cell cluster using a Tfh13-associated gene signature. This approach identified two transcriptionally distinct subpopulations enriched for either Tfh13 or cTfh cell gene programs (Figure 4C). Notably, the Tfh13 signature-enriched subset expressed elevated levels of *Ltb4r1*, *Il5*, and *Il13*, consistent with commitment to the Tfh13 lineage (Figure 4D). By contrast, the cTfh signature-enriched subpopulation was characterized by increased expression of Il21, a hallmark of mature cTfh cells (Figure 4D). The remaining proliferative T cells lacked distinct lineage-defining transcriptional profiles, suggesting retention of bipotent differentiation potential or the capacity for memory T cell development. These results suggest heterogeneity within the proliferative T cell subset, with distinct developmental potentials.

LTB4-Ltb4r1 signaling promotes type 2 cytokine transcription in Tfh13 cells

During allergic responses, antigen-specific IgE crosslinking of FcεRI on mast cells and basophils induces the release of inflammatory and vasoactive mediators, including LTB4. In line with the hyper-IgE phenotype observed in T-*Bach2*$^{-/-}$ mice, we detected elevated LTB4 concentrations in the serum, BALF, and medLNs (Figure 5A), indicative of active LTB4-Ltb4r1 signaling in Tfh13 cells. Next, we investigated how Ltb4r1 signaling shapes Tfh13 cell phenotypes. Previous studies have implicated Ltb4r1 in the amplification of allergic airway inflammation.[35–37] In particular, genetic ablation of *Ltb4r1* has been shown to impair type 2 cytokine production and diminish IgE responses in murine models of allergy,[37,38] supporting a model in which Ltb4r1 upregulation enhances type 2 polarization in Tfh13 cells.

To investigate whether LTB4-Ltb4r1 signaling promotes type 2 polarization in Tfh cells, we isolated Tfh cells from WT and *Bach2*-deficient mice and stimulated them with LTB4. As previously reported, Bach2 deficiency upregulates the transcription of *Cxcr5*, *Il4*, *Il13*, and *Gata3*.[22,23] LTB4 treatment further increased the expression of *Il4*, *Il5*, *Il13*, and *Gata3* in *Bach2*-deficient Tfh cells but had no appreciable effect in *Bach2*-sufficient controls (Figure 5B). Notably, Cxcr5 expression remained unchanged upon LTB4 treatment, indicating that LTB4 selectively promotes the type 2 transcriptional program rather than general Tfh identity. Notably, LTB4 also induced Ltb4r1 expression in *Bach2*-deficient Tfh cells, but not controls (Figure 5B), suggesting a feedforward loop normally constrained by Bach2. Using available chromatin immunoprecipitation sequencing (ChIP-seq) data in activated CD4$^+$ T cells,[25] we found that BACH2 bound to the *Ltb4r1* genomic locus (Figure 5C). This binding was further validated by ChIP followed by qPCR in Tfh-like cells (Figure 5C). Given the near-complete absence of Bach2 expression in WT Tfh13 cells (Figure 3G), we propose that Bach2 downregulation is a prerequisite for LTB4-induced Ltb4r1 expression and the subsequent amplification of type 2 cytokine transcription in Tfh13 cells.

To assess the relevance of this regulatory axis in human cells, we silenced BACH2 in human tonsil-derived CXCR5$^+$PD1$^+$ Tfh cells using a pool of small interfering RNA (siRNA) against *BACH2* (Figure 5D). The siRNA pool was co-transfected with GFP-encoding mRNA at a 1:1 ratio, and GFP$^+$ cells were sorted for downstream analysis. BACH2 knockdown alone modestly increased type 2 cytokine transcript levels, although this effect did not reach statistical significance (Figure 5E). However, LTB4 treatment markedly enhanced *IL4*, *IL5*, and *IL13* mRNA levels specifically in BACH2-silenced cells, with no such induction observed in BACH2-sufficient controls (Figure 5E). These findings highlight a conserved role for LTB4-Ltb4r1 signaling in

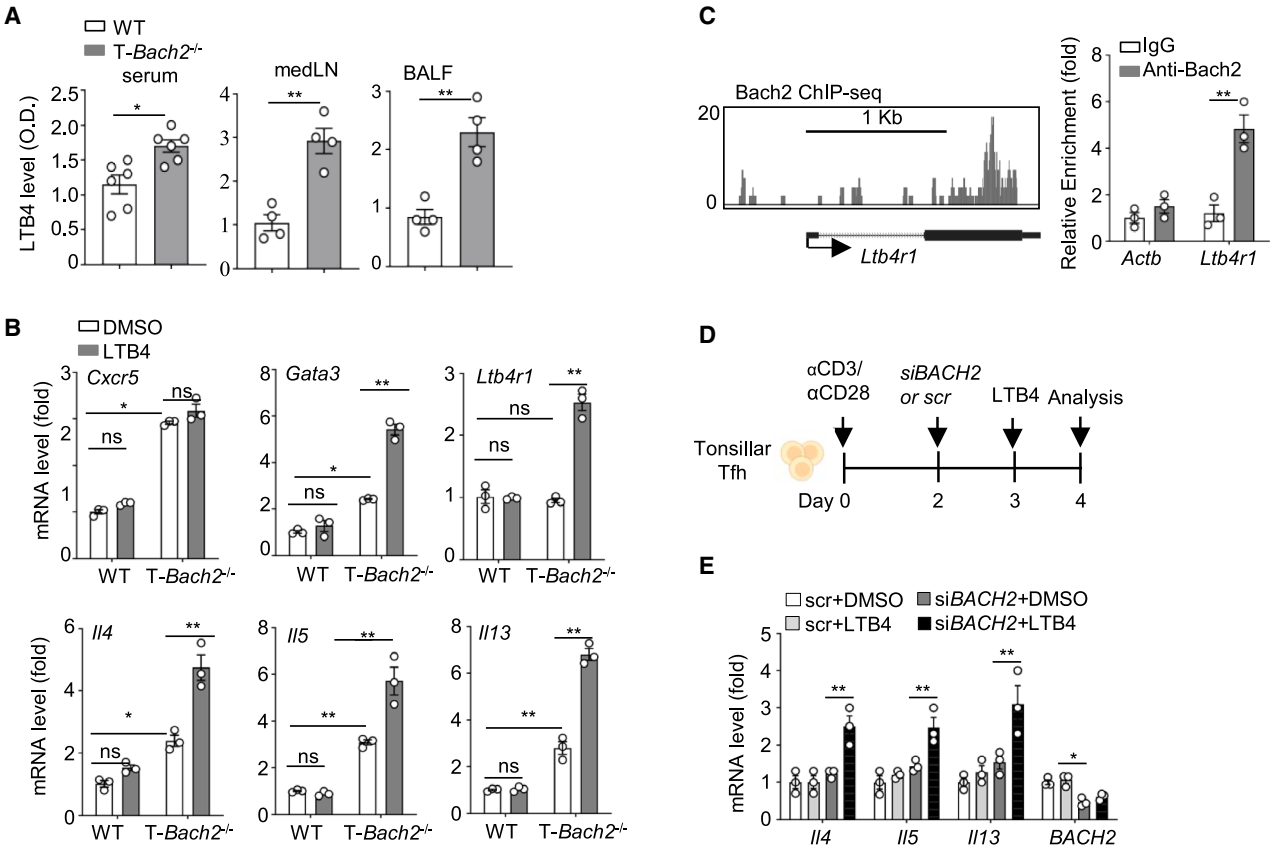

Figure 5. Bach2 suppresses the LTB4-Ltb4r1 axis to repress the type 2 cytokine transcription

(A) Relative levels of LTB4 in the serum, medLNs, and BALF in WT and T-*Bach2*$^{-/-}$ mice following LPS+OVA immunization, measured by ELISA. O.D., optical density.

(B) RT-qPCR analysis of mRNA levels of indicated genes in isolated mouse Tfh cells treated with 0.1 mM LTB4 or DMSO for 24 h.

(C) Illustration depicting ChIP-seq tracks of Bach2 at the *Ltb4r1* gene locus in activated CD4^{+} T cells by bioinformatics analysis of a published dataset (GEO: GSE65084). The right image depicts the relative enrichment of Bach2 binding at the indicated loci in Tfh-like cells, accessed by ChIP-qPCR.

(D) Schematic of experimental design for siRNA-mediated knockdown of BACH2 in Tfh cells isolated from human tonsils.

(E) RT-qPCR analysis of mRNA levels of indicated genes in *BACH2*-knockdown human Tfh cells isolated from tonsils and cultured under different conditions.

In (B) and (E), data are represented as the fold change relative to DMSO-treated WT cells after normalization with *Actb*. In (A)–(C) and (E), data are presented as the means ± SEM and are representative of at least two independent experiments. ns, not significant; *$p < 0.05$, and **$p < 0.01$ by two-tailed *t* test (C) or one-way ANOVA (B and E).

promoting type 2 cytokine expression in Tfh13 cells in the context of BACH2 deficiency, underscoring the relevance of this pathway in human Tfh13 cell regulation.

Ltb4r1 inhibitor impairs Tfh13 cell development in T-*Bach2*$^{-/-}$ mice

To further assess the role of Ltb4r1 in Tfh13 cell formation *in vivo*, 6- to 8-week-old T-*Bach2*$^{-/-}$ mice were intragastrically treated with the Ltb4r1 antagonist CP105696 (100 mg/kg) or vehicle control seven times throughout the course of LPS+OVA immunization to inhibit LTB4-Ltb4r1 signaling (Figure S5A). Pharmacological blockade of Ltb4r1 significantly reduced the frequencies of both total Tfh cells and Tfh13 cells in the medLNs, with a more pronounced reduction observed in the Tfh13 subset (Figure S5B). A modest trend toward decreased GC B cell proportions was also observed following Ltb4r1 inhibition (Figure S5C). These findings suggest that Tfh13 cells exhibit heightened sensitivity to LTB4-LTB Ltb4r14R1 signaling *in vivo*.

Consistent with impaired Tfh13 cell responses, Ltb4r1 inhibition led to a significant reduction in both total and high-affinity NP-binding IgE levels in the serum and BALF (Figure S5D). Moreover, Ltb4r1 inhibition substantially attenuated inflammatory cell infiltration and mucus production in the lungs of T-*Bach2*$^{-/-}$ mice (Figure S5E). Together, these results identify the LTB4-Ltb4r1 signaling axis as a key regulator of Tfh13 cell differentiation and allergic inflammation *in vivo*.

Genetic ablation of Ltb4r1 in T cells selectively impairs Tfh13 cell development

Ltb4r1 is expressed by a variety of immune and non-immune cell types.[35,36] To determine whether the impaired Tfh13 cell differentiation observed upon Ltb4r1 blockade results from cell-intrinsic effects in T cells, we generated T cell-specific

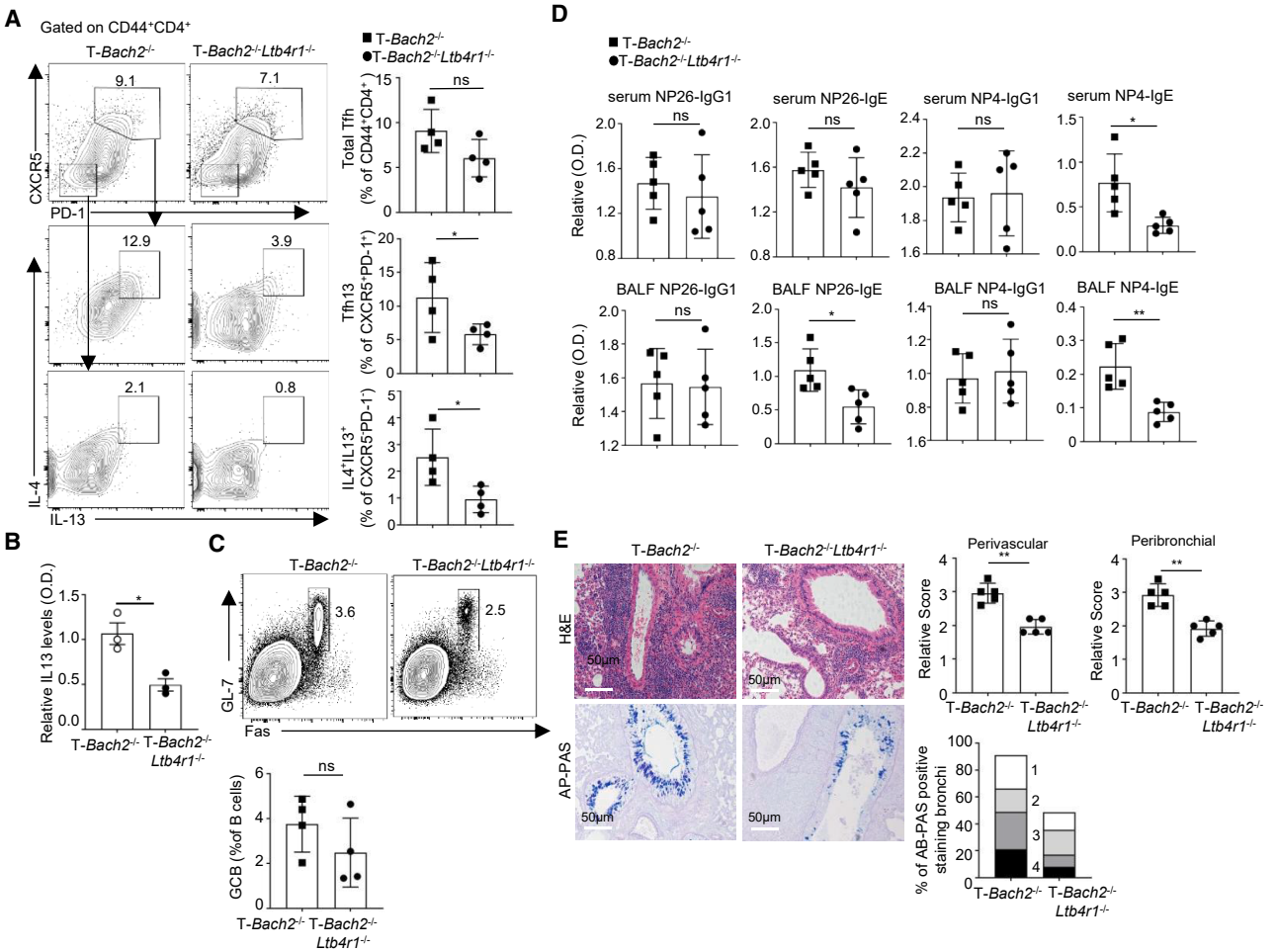

Figure 6. Ltb4r1 deficiency impairs Tfh13 cell formation and high-affinity IgE production in T-*Bach2*$^{-/-}$ mice

(A–D) 6- to 8-week-old T-*Bach2*$^{-/-}$ and T-*Bach2*$^{-/-}$*Ltb4r1*$^{-/-}$ mice were subjected for analysis post LPS+OVA immunization.

(A) Representative flow plots and quantifications showing the frequencies of total CXCR5^{+}PD1^{+} Tfh cells among CD44^{+}CD4^{+} T cells, IL-4^{+}IL-13^{+} Tfh13 cells among total Tfh cells, and IL-4^{+}IL-13^{+} cells among non-Tfh cells.

(B) Relative levels of IL-13 in the supernatant from T-*Bach2*$^{-/-}$ and T-*Bach2*$^{-/-}$*Ltb4r1*$^{-/-}$ Tfh cells stimulated with anti-CD3 and anti-CD28 antibodies *in vitro*, measured by ELISA.

(C) Representative flow plots and summary data showing the frequencies of Fas^{+}GL7^{+} GC B cells among CD19^{+} B cells.

(D) Relative levels of high-affinity NP4-binding and total NP26-binding IgE in the serum and BALF.

(E) Representative H&E and AB-PAS staining of lung sections. Scale bars: 50 μm. Quantifications of perivascular and peribronchial inflammation, as well as goblet cell metaplasia, are shown at the bottom.

Each symbol represents one mouse. Data are presented as the means ± SEM and are representative of at least two independent experiments. ns, not significant; *$p < 0.05$ and **$p < 0.01$ by two-tailed *t* test. See also Figure S5.

Ltb4r1-deficient mice (T- *Ltb4r1*$^{-/-}$). T- *Ltb4r1*$^{-/-}$ mice displayed normal frequencies of activated CD4^{+} T cells and total Tfh cells following LPS+OVA immunization (Figures S6A and S6B). Similar to WT controls, T-*Ltb4r1*$^{-/-}$ mice failed to generate Tfh13 cells or produce high-affinity IgE in response to LPS+OVA (Figures S6B and S6C). These results indicate that Ltb4r1 is dispensable for the type 1 immune response induced by LPS+OVA in WT mice.

We next assessed the effects of *Ltb4r1* deficiency on Tfh13 responses in *Bach2*-deficient mice following LPS+OVA immunization. To this end, we generated T cell-specific knockout mice for both Bach2 and Ltb4r1 (T-*Bach2*$^{-/-}$*Ltb4r1*$^{-/-}$). Following LPS+OVA immunization, T-*Bach2*$^{-/-}$*Ltb4r1*$^{-/-}$ mice exhibited comparable total Tfh cell proportions with T-*Bach2*$^{-/-}$ mice (Figure 6A) but a reduction of IL-13 secretion (Figure 6B). Accordingly, IL-4^{+}IL-13^{+} Tfh13 cell proportions were significantly reduced in the absence of Ltb4r1 (Figure 6A), indicating a selective requirement for Ltb4r1 in this subset. GC B cell frequencies were largely unchanged (Figure 6C).

ELISA further revealed that *Ltb4r1* ablation did not significantly alter total or high-affinity NP-binding IgG1 levels in the serum and BALF of T-*Bach2*$^{-/-}$ mice (Figure 6D). However, high-affinity NP-binding IgE levels were markedly diminished in both compartments of T-*Bach2*$^{-/-}$*Ltb4r1*$^{-/-}$ mice compared to

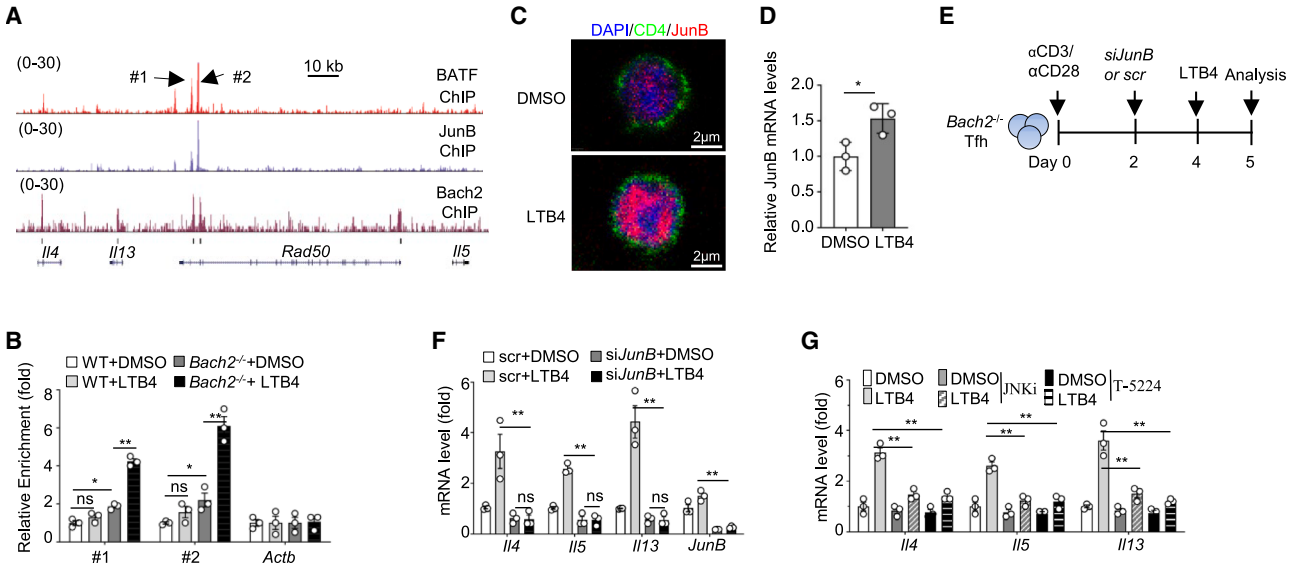

Figure 7. Bach2 antagonizes the LTB4-Ltb4r1-JunB axis to repress type 2 cytokine production

(A) Illustration depicting ChIP-seq tracks of Bach2, JunB, and BATF at type 2 cytokine gene loci in activated CD4$^+$ T cells, analyzed using published datasets (GEO: GSE65084 and GSE121295). Co-occupancy of JunB and Bach2 at two AP-1 motifs #1 and #2 is indicated by arrows.

(B) The relative enrichment of JunB binding at indicated loci in WT and *Bach2*-deficient Tfh-like cells treated with 0.1 μM LTB4 or DMSO.

(C) Representative immunofluorescence staining of *Bach2*-deficient Tfh-like cells treated with 0.1 μM LTB4 or DMSO. Nuclei counterstained with DAPI. Scale bars: 2 μm.

(D) RT-qPCR analysis of *JunB* mRNA levels in *Bach2*-deficient Tfh-like cells treated with 0.1 μM LTB4 or DMSO.

(E) Schematic of experimental design for siRNA-mediated knockdown of JunB in Tfh cells isolated from T-*Bach2*$^{-/-}$ mice.

(F) RT-qPCR analysis of mRNA levels of indicated genes in *Bach2*-deficient Tfh cells transfected with a pool of siRNA against *JunB* and cultured with or without 0.1 μM LTB4.

(G) RT-qPCR analysis of mRNA levels of indicated genes in *Bach2*-deficient Tfh cells pretreated with 10 μM JNK inhibitor or 50 μM AP-1 inhibitor (T-5224) for 1 h before 0.1 μM LTB4 stimulation for 24 h.

Data are presented as the means ± SEM and are representative of at least two independent experiments. ns, not significant; *$p < 0.05$ and **$p < 0.01$ by two-tailed *t* test (D) or one-way ANOVA (B, F, and G). See also Figure S6.

T-*Bach2*$^{-/-}$ controls (Figure 6D). Total NP-specific IgE in the BALF was also modestly but significantly decreased, whereas serum IgE levels remained unaffected (Figure 6D). Histological analysis demonstrated that *Ltb4r1* deficiency substantially alleviated lung immune cell infiltration and mucus hypersecretion in T-*Bach2*$^{-/-}$ mice (Figure 6E). Global *Ltb4r1* deficiency has been associated with reduced type 2 cytokine production and IgE levels in Th2-type allergic models,[38,39] and type 2 allergen HDM was able to induce Tfh13 cells.[12] Thus, we asked whether Ltb4r1 deficiency in T cells could limit a Tfh13 response. We observed that T-*Ltb4r1*$^{-/-}$ mice exhibited lower levels of Tfh13 cells and high-affinity IgE compared to WT mice following HDM immunization (Figures S6D and S6E). Together, these findings identify Ltb4r1 as a critical regulator of Tfh13 cell development and high-affinity IgE production.

Ltb4r1 signaling activates JunB to amplify type 2 cytokine transcription in the absence of Bach2

To elucidate the mechanism by which LTB4-Ltb4r1 signaling enhances type 2 cytokine expression in Tfh13 cells, we focused on the AP-1 transcription factor JunB, which is known to activate the Il4 promoter and drive Th2 cytokine transcription.[40,41] JunB is both upregulated in Tfh13 cells and required for their differentiation.[16] LTB4 has been shown to induce phosphorylation of c-Jun N-terminal kinase (JNK), a known upstream activator of JunB, in human lymphocytes and murine macrophages.[42,43] Based on these observations, we hypothesized that LTB4-Ltb4r1 signaling promotes type 2 cytokine expression in Tfh13 cells through activation of the JNK-JunB axis.

The Bach2-Batf complex is known to suppress type 2 cytokine transcription by binding AP-1 motifs within type 2 cytokine loci.[25] Analysis of public ChIP-seq data revealed co-occupancy of JunB and Bach2 at two distinct AP-1 motifs in activated CD4$^+$ T cells (Figure 7A).[25,44] In the absence of Bach2, JunB binding at these sites increased (Figure 7B), suggesting competitive and antagonistic regulation between the two factors. This model was functionally supported by LTB4 treatment, which further enhanced JunB occupancy at these sites in *Bach2*$^{-/-}$ but not WT Tfh-like cells (Figure 7B). Additionally, LTB4 stimulation increased *Junb* transcript abundance and JunB protein levels (Figures 7C and 7D), indicating that LTB4-Ltb4r1 signaling not only promotes JunB binding but also upregulates its expression, thereby establishing a positive feedback mechanism to amplify type 2 cytokine transcription.

To determine whether JunB is required for LTB4-mediated induction of type 2 cytokine transcription in *Bach2*$^{-/-}$ Tfh13 cells, we performed siRNA-mediated knockdown of JunB in *Bach2*-deficient Tfh-like cells (Figure 7E). A pool of JunB-targeting

siRNAs was co-transfected with GFP-encoding mRNA, and GFP$^+$ cells were sorted for downstream analysis. JunB silencing markedly impaired the LTB4-induced upregulation of type 2 cytokine transcripts (Figure 7F), indicating a critical role for JunB in this process. Consistently, pharmacological inhibition of JNK signaling or blockade of AP-1 DNA-binding activity using T-5224 similarly abrogated LTB4-induced type 2 cytokine expression in *Bach2*$^{-/-}$ Tfh-like cells (Figure 7G). Together, these findings demonstrate that LTB4-Ltb4r1 signaling drives type 2 cytokine transcription via the JNK-JunB axis and that Bach2 antagonizes this pathway by repressing JunB activity through competitive binding at AP-1 motifs.

DISCUSSION

The molecular circuits governing Tfh13 cell development remain poorly understood. Here, we identify Bach2 as a critical transcriptional repressor that constrains Tfh13 cell formation. *Bach2*-deficient mice exhibited a significant expansion of Tfh13 cells, even under conditions that typically do not induce their differentiation. This expansion was accompanied by elevated levels of high-affinity IgE and severe allergic airway inflammation. While JunB has been established as a key transcriptional activator of Tfh13 cell development,[16] we identified the LTB4-Ltb4r1 axis as an upstream regulator promoting JunB-dependent Tfh13 differentiation. Mechanistically, Bach2 directly antagonizes JunB to repress type 2 cytokine gene expression, a defining feature of Tfh13 cell effector function. Our findings reveal an antagonistic regulatory network comprising Bach2-mediated repression and LTB4-Ltb4r-JunB-driven activation that orchestrates Tfh13 cell development.

Tfh13 cells constitute a transcriptionally distinct subset that diverges from conventional Tfh cells,[12] yet their defining transcriptional signatures remain elusive. While previous studies have shown that Tfh13 cells express elevated levels of type 2 cytokines,[12] our findings further demonstrate that their gene expression profile more closely resembles that of GC-resident Tfh cells than cTfh cells, accompanied by altered niche positioning. We identify CXCR6 as a defining surface marker of GC-resident Tfh cells and show that Tfh13 cells upregulate CXCR6 to a greater extent than other Tfh subsets. These results suggest that Tfh13 cells preferentially localize to the GC, potentially endowing them with an enhanced capacity to support B cell responses. The functional contribution of CXCR6 in guiding Tfh13 cell positioning within the GC niche warrants further investigation.

Accumulating evidence has shown that Tfh cell subsets exhibit considerable plasticity and interconversion during both primary immune responses and memory recall.[4,10,33,34] The ontogeny and developmental pathways of Tfh13 cells in our model are likely to be complex. We observed that Tfh13 cells shared a substantial proportion of TCRs with both cTfh cells and proliferative T cells. Within the proliferative T cell compartment, we identified a transcriptionally distinct subset marked by high expression of type 2 cytokines and Ltb4r1, suggesting a potential commitment to the Tfh13 lineage. Circulating or tissue-resident memory T cells and Th2 cells can convert into effector cTfh cells under some conditions.[4,10,34] Accordingly, we speculate that memory T cells and Th2 cells generated during the sensitization phase may convert into Tfh13 cells during allergen re-exposure in our model. Therefore, we propose that Tfh13 cells observed on day 27 in our model may comprise those initially generated during the sensitization phase, as well as those transitioning from memory Tfh cells and Th2 cells during allergen rechallenge, or those directly derived from the Tfh13-committed proliferative compartment.

A pivotal finding of this study is the identification of the LTB4-Ltb4r1 axis as a critical mediator of Tfh13 cell differentiation. We show that Bach2 downregulation in Tfh13 cells permits the upregulation of Ltb4r1, thereby conferring responsiveness to LTB4 released by IgE-activated mast cells and basophils during allergic inflammation. The functional importance of this pathway was validated *in vivo* through pharmacological inhibition of Ltb4r1 and genetic ablation of Ltb4r1 in T cells, both of which led to a marked reduction in Tfh13 cell frequency. Mechanistically, we pinpoint JunB as a critical downstream effector of LTB4-Ltb4r1 signaling. JunB, previously implicated in promoting Th2 cytokine expression[40,41] and required for Tfh13 cell fate commitment,[16] was found to bind type 2 cytokine loci at AP-1 motifs co-occupied by Bach2. LTB4 stimulation enhanced JunB occupancy at these sites specifically in *Bach2*-deficient Tfh-like cells, indicating that Bach2 antagonizes JunB-mediated transcriptional activation by competing for shared regulatory elements. This interaction establishes Bach2 as a molecular gatekeeper that restrains JunB-dependent type 2 cytokine expression and thereby Tfh13 differentiation. Although Ltb4r1 deficiency significantly impaired Tfh13 development in *Bach2*-deficient mice, it did not fully abrogate it. Given that Ltb4r1 signaling is engaged primarily during the antigen challenge phase via IgE-FcεRI-mediated LTB4 release, while high-affinity IgE production can occur during the initial sensitization phase, our findings support a two-step model of Tfh13 cell differentiation. In this model, Bach2 loss initiates Tfh13 development and an early surge of high-affinity IgE during the sensitization phase. Upon subsequent allergen exposure, LTB4 released by FcεRI-crosslinked mast cells and basophils activates the Ltb4r1-JunB pathway to reinforce Tfh13 polarization and sustain high-affinity IgE production. Together, these findings delineate a feedforward circuit wherein Bach2 loss licenses IgE-LTB_4-Ltb4r1-JunB signaling to drive Tfh13 cell differentiation and function in our model. We also observed that Ltb4r1 deficiency in T cells impaired the Tfh13 response induced by the type 2 allergen HDM, most likely due to the near-complete absence of Bach2 expression in these cells. This regulatory loop provides a mechanistic rationale for targeting Ltb4r1 in Tfh13-associated allergic disease. Notably, this pathway appears conserved in Th2 cells, which also express high levels of Ltb4r1.[45] In line with this, genetic ablation of Ltb4r1 in Bach2-deficient mice significantly reduced IL-4$^+$IL-13$^+$ Th2 cell frequencies, further supporting the broader relevance of this pathway across type 2 effector populations.

Bach2 is a well-established suppressor of type 2 immune responses by inhibiting the development of Th2 cells and IL-4-producing Tfh2 cells under both immunized and steady-state conditions.[22,25] Here, we identify Bach2 as a critical checkpoint that constrains both induced and spontaneous Tfh13 cell

responses under type 1 immune and steady-state conditions, respectively, thereby reinforcing its broad role as a transcriptional repressor of type 2 immunity. We propose that during allergen-induced type 2 immune responses, a subset of $CD4^+$ T cells undergo marked downregulation of Bach2, licensing their differentiation into Tfh13 cells. Notably, genetic polymorphisms at the human *BACH2* locus are associated with increased susceptibility to allergic diseases, including asthma,[17] and may impair BACH2 expression or function in T cells, predisposing individuals to a Tfh13-skewed phenotype. Our findings suggest that aberrant induction of pathogenic Tfh13 cells may underlie allergic disease pathogenesis in human carriers of BACH2 variants.

In summary, we identify Bach2 as a pivotal transcriptional repressor that limits Tfh13 cell differentiation, thereby preventing excessive high-affinity IgE production and allergic airway inflammation. Our findings uncover the LTB4-Ltb4r1-JunB signaling axis as a key driver of Tfh13 cell fate and effector function, providing mechanistic insight into the transcriptional and environmental cues that govern IgE-mediated immune responses. These results advance our understanding of the molecular circuitry underpinning allergic disease and identify potential therapeutic targets for the treatment of Tfh13-driven IgE-mediated disorders.

Limitations of the study

Bach2 deficiency can broadly affect $CD4^+$ T cell differentiation, enhancing a biased Th2 program and Tfh cell differentiation, which may influence Tfh13 development. Bach2 antagonizes LTB4-JunB signaling to restrain type 2 cytokine production in mature human and murine Tfh cells *in vitro*, suggesting a Tfh-intrinsic role for Bach2 in suppressing Tfh13 polarization. Inducible deletion of Bach2 in $CXCR5^+$ T cells would provide valuable insights into the specific effects of Bach2 on Tfh13 development, as well as the relationship between Tfh13 expansion and skewed type 2 cytokine production in the absence of Bach2. Given the multiple developmental origins of Tfh13 cells in our model, approaches such as OT-II cell adoptive transfer could offer valuable perspectives on the ontogeny and differentiation of Tfh13 cells.

RESOURCE AVAILABILITY

Lead contact

Further information and requests for resources and reagents should be directed to and will be fulfilled by the lead contact, Chuanxin Huang (huangcx@shsmu.edu.cn).

Materials availability

All unique reagents generated in this study are available from the lead contact with a completed materials transfer agreement.

Data and code availability

- The scRNA-seq data have been deposited at the National Genomics Data Center (https://ngdc.cncb.ac.cn/) under the accession number CRA016485 and are publicly available as of the date of publication.
- This paper does not report original code.
- Any additional information required to reanalyze the data reported in this work paper is available from the lead contact upon request.

ACKNOWLEDGMENTS

This work was supported by the National Key R&D Program of China (2021YFA1301403), the National Natural Science Foundation of China (32470932, 82270027, 82301969, 32200741, and 82371745), the Shanghai Municipal Health Commission (202140097), the Innovative Research Team of High-level Local Universities in Shanghai, and the Shanghai Frontiers Science Center of Cellular Homeostasis and Human Diseases.

AUTHOR CONTRIBUTIONS

Conceptualization, C.H. and W.Z.; investigation, L.Z. and H.Z.; validation, Q.H. and M.Z.; writing – original draft, C.H. and W.Z.; writing – review & editing, C.H.; funding acquisition, C.H. and W.Z.; supervision, C.H.

DECLARATION OF INTERESTS

All authors declare no competing interests.

STAR★METHODS

Detailed methods are provided in the online version of this paper and include the following:

- KEY RESOURCES TABLE
- EXPERIMENTAL MODEL AND STUDY PARTICIPANT DETAILS
  - Mouse models
- METHOD DETAILS
  - Immunization
  - Flow cytometry and cell sorting
  - *In vivo* treatment of Ltb4r1 inhibitor
  - *In vitro* Tfh-like cell differentiation and inhibitor treatment
  - siRNA knockdown and inhibitor treatment in Tfh cells cultured *in vitro*
  - Quantitative PCR (QPCR)
  - *In vitro* Tfh-like cell differentiation
  - Chromatin immunoprecipitation (ChIP)-QPCR analysis
  - Enzyme-linked immunosorbent assay (ELISA)
  - Histological analysis
  - Immunofluorescence
  - Single-cell RNA-sequencing (scRNA-seq) and data analysis
  - scTCR-seq
- QUANTIFICATION AND STATISTICAL ANALYSIS

SUPPLEMENTAL INFORMATION

Supplemental information can be found online at https://doi.org/10.1016/j.celrep.2026.117220.

Received: August 12, 2025
Revised: December 14, 2025
Accepted: March 16, 2026
Published: April 7, 2026

REFERENCES

1. Cruz, A.A., Cooper, P.J., Figueiredo, C.A., Alcantara-Neves, N.M., Rodrigues, L.C., and Barreto, M.L. (2017). Global issues in allergy and immunology: Parasitic infections and allergy. J. Allergy Clin. Immunol. *140*, 1217–1228. https://doi.org/10.1016/j.jaci.2017.09.005.
2. Oettgen, H.C., and Geha, R.S. (2001). IgE regulation and roles in asthma pathogenesis. J. Allergy Clin. Immunol. *107*, 429–440. https://doi.org/10.1067/mai.2001.113759.
3. Mita, H., Yasueda, H., and Akiyama, K. (2000). Affinity of IgE antibody to antigen influences allergen-induced histamine release. Clin. Exp. Allergy *30*, 1583–1589. https://doi.org/10.1046/j.1365-2222.2000.00921.x.

4. Ballesteros-Tato, A., Randall, T.D., Lund, F.E., Spolski, R., Leonard, W.J., and León, B. (2016). T Follicular Helper Cell Plasticity Shapes Pathogenic T Helper 2 Cell-Mediated Immunity to Inhaled House Dust Mite. Immunity *44*, 259–273. https://doi.org/10.1016/j.immuni.2015.11.017.

5. Kobayashi, T., Iijima, K., Dent, A.L., and Kita, H. (2017). Follicular helper T cells mediate IgE antibody response to airborne allergens. J. Allergy Clin. Immunol. *139*, 300–313.e7. https://doi.org/10.1016/j.jaci.2016.04.021.

6. Dolence, J.J., Kobayashi, T., Iijima, K., Krempski, J., Drake, L.Y., Dent, A.L., and Kita, H. (2018). Airway exposure initiates peanut allergy by involving the IL-1 pathway and T follicular helper cells in mice. J. Allergy Clin. Immunol. *142*, 1144–1158.e8. https://doi.org/10.1016/j.jaci.2017.11.020.

7. Olatunde, A.C., Hale, J.S., and Lamb, T.J. (2021). Cytokine-skewed Tfh cells: functional consequences for B cell help. Trends Immunol. *42*, 536–550. https://doi.org/10.1016/j.it.2021.04.006.

8. Weinstein, J.S., Herman, E.I., Lainez, B., Licona-Limón, P., Esplugues, E., Flavell, R., and Craft, J. (2016). TFH cells progressively differentiate to regulate the germinal center response. Nat. Immunol. *17*, 1197–1205. https://doi.org/10.1038/ni.3554.

9. Podestà, M.A., Cavazzoni, C.B., Hanson, B.L., Bechu, E.D., Ralli, G., Clement, R.L., Zhang, H., Chandrakar, P., Lee, J.-M., Reyes-Robles, T., et al. (2023). Stepwise differentiation of follicular helper T cells reveals distinct developmental and functional states. Nat. Commun. *14*, 7712. https://doi.org/10.1038/s41467-023-43427-4.

10. Feng, H., Zhao, Z., Zhao, X., Bai, X., Fu, W., Zheng, L., Kang, B., Wang, X., Zhang, Z., and Dong, C. (2024). A novel memory-like Tfh cell subset is precursor to effector Tfh cells in recall immune responses. J. Exp. Med. *221*, e20221927.

11. Gowthaman, U., Sikder, S., Lee, D., and Fisher, C. (2022). T follicular helper cells in IgE-mediated pathologies. Curr. Opin. Immunol. *74*, 133–139. https://doi.org/10.1016/j.coi.2021.12.001.

12. Gowthaman, U., Chen, J.S., Zhang, B., Flynn, W.F., Lu, Y., Song, W., Joseph, J., Gertie, J.A., Xu, L., Collet, M.A., et al. (2019). Identification of a T follicular helper cell subset that drives anaphylactic IgE. Science *365*, eaaw6433. https://doi.org/10.1126/science.aaw6433.

13. Tong, X., Guan, C., Ji, T., Cao, C., Jiang, J., Liu, M., Guo, Q., Zhou, P., and Gong, F. (2022). Increased circulating T follicular helper 13 subset correlates with high IgE levels in pediatric allergic asthma. Eur. J. Immunol. *52*, 2010–2012. https://doi.org/10.1002/eji.202250076.

14. Lozano-Ojalvo, D., Chen, X., Kazmi, W., Menchén-Martínez, D., Pérez-Rodríguez, L., Fernandes-Braga, W., Tyler, S., Benkov, K., Pittman, N., Lai, J., et al. (2025). Differential T follicular helper cell phenotypes distinguish IgE-mediated milk allergy from eosinophilic esophagitis in children. J. Allergy Clin. Immunol. *155*, 909–922. https://doi.org/10.1016/j.jaci.2024.09.024.

15. Chen, J.S., Grassmann, J.D.S., Gowthaman, U., Olyha, S.J., Simoneau, T., Berin, M.C., Eisenbarth, S.C., and Williams, A. (2021). Flow cytometric identification of T 13 cells in mouse and human. J. Allergy Clin. Immunol. *147*, 470–483. https://doi.org/10.1016/j.jaci.2020.04.063.

16. Chandrakar, P., Nelson, C.S., Podestà, M.A., Cavazzoni, C.B., Gempler, M., Lee, J.-M., Richardson, S., Zhang, H., Samarpita, S., Ciofani, M., et al. (2025). Progressively differentiated TFH13 cells are stabilized by JunB to mediate allergen germinal center responses. Nat. Immunol. *26*, 473–483. https://doi.org/10.1038/s41590-025-02077-y.

17. Ferreira, M.A.R., Matheson, M.C., Duffy, D.L., Marks, G.B., Hui, J., Le Souëf, P., Danoy, P., Baltic, S., Nyholt, D.R., Jenkins, M., et al. (2011). Identification of IL6R and chromosome 11q13.5 as risk loci for asthma. Lancet *378*, 1006–1014. https://doi.org/10.1016/s0140-6736(11)60874-x.

18. Richer, M.J., Lang, M.L., and Butler, N.S. (2016). T Cell Fates Zipped Up: How the Bach2 Basic Leucine Zipper Transcriptional Repressor Directs T Cell Differentiation and Function. J. Immunol. *197*, 1009–1015. https://doi.org/10.4049/jimmunol.1600847.

19. Roychoudhuri, R., Hirahara, K., Mousavi, K., Clever, D., Klebanoff, C.A., Bonelli, M., Sciumè, G., Zare, H., Vahedi, G., Dema, B., et al. (2013). BACH2 represses effector programs to stabilize Treg-mediated immune homeostasis. Nature *498*, 506–510. https://doi.org/10.1038/nature12199.

20. Tsukumo, S.-i., Unno, M., Muto, A., Takeuchi, A., Kometani, K., Kurosaki, T., Igarashi, K., and Saito, T. (2013). Bach2 maintains T cells in a naive state by suppressing effector memory-related genes. Proc. Natl. Acad. Sci. USA *110*, 10735–10740. https://doi.org/10.1073/pnas.1306691110.

21. Yu, X., Lao, Y., Teng, X.L., Li, S., Zhou, Y., Wang, F., Guo, X., Deng, S., Chang, Y., Wu, X., et al. (2018). SENP3 maintains the stability and function of regulatory T cells via BACH2 deSUMOylation. Nat. Commun. *9*, 3157.

22. Zhang, H., Hu, Q., Zhang, M., Yang, F., Peng, C., Zhang, Z., and Huang, C. (2019). Bach2 Deficiency Leads to Spontaneous Expansion of IL-4-Producing T Follicular Helper Cells and Autoimmunity. Front. Immunol. *10*, 2050. https://doi.org/10.3389/fimmu.2019.02050.

23. Geng, J., Wei, H., Shi, B., Wang, Y.-H., Greer, B.D., Pittman, M., Smith, E., Thomas, P.G., Kutsch, O., and Hu, H. (2019). Bach2 Negatively Regulates T Follicular Helper Cell Differentiation and Is Critical for CD4+ T Cell Memory. J. Immunol. *202*, 2991–2998. https://doi.org/10.4049/jimmunol.1801626.

24. Lahmann, A., Kuhrau, J., Fuhrmann, F., Heinrich, F., Bauer, L., Durek, P., Mashreghi, M.-F., and Hutloff, A. (2019). Bach2 Controls T Follicular Helper Cells by Direct Repression of Bcl-6. J. Immunol. *202*, 2229–2239. https://doi.org/10.4049/jimmunol.1801400.

25. Kuwahara, M., Ise, W., Ochi, M., Suzuki, J., Kometani, K., Maruyama, S., Izumoto, M., Matsumoto, A., Takemori, N., Takemori, A., et al. (2016). Bach2–Batf interactions control Th2-type immune response by regulating the IL-4 amplification loop. Nat. Commun. *7*, 12596. https://doi.org/10.1038/ncomms12596.

26. Yu, B., Pei, C., Peng, W., Zheng, Y., Fu, Y., Wang, X., Wang, W., Wang, Z., Chen, Y., Wang, Q., et al. (2025). Microbiota-derived butyrate alleviates asthma via inhibiting Tfh13-mediated IgE production. Signal Transduct Tar *10*, 181.

27. Zhang, H., Dai, D., Hu, Q., Yang, F., Xue, Y., Li, F., Shen, N., Zhang, M., and Huang, C. (2021). Bach2 attenuates IL-2R signaling to control Treg homeostasis and Tfr development. Cell Rep. *35*, 109096.

28. Clement, R.L., Daccache, J., Mohammed, M.T., Diallo, A., Blazar, B.R., Kuchroo, V.K., Lovitch, S.B., Sharpe, A.H., and Sage, P.T. (2019). Follicular regulatory T cells control humoral and allergic immunity by restraining early B cell responses. Nat. Immunol. *20*, 1360–1371. https://doi.org/10.1038/s41590-019-0472-4.

29. Kim, E.H., Gasper, D.J., Lee, S.H., Plisch, E.H., Svaren, J., and Suresh, M. (2014). Bach2 Regulates Homeostasis of Foxp3+ Regulatory T Cells and Protects against Fatal Lung Disease in Mice. J. Immunol. *192*, 985–995. https://doi.org/10.4049/jimmunol.1302378.

30. Mabrouk, N., Tran, T., Sam, I., Pourmir, I., Gruel, N., Granier, C., Pineau, J., Gey, A., Kobold, S., Fabre, E., and Tartour, E. (2022). CXCR6 expressing T cells: Functions and role in the control of tumors. Front. Immunol. *13*, 1022136.

31. Yeh, C.-H., Finney, J., Okada, T., Kurosaki, T., and Kelsoe, G. (2022). Primary germinal center-resident T follicular helper cells are a physiologically distinct subset of CXCR5hiPD-1hi T follicular helper cells. Immunity *55*, 272–289.e7. https://doi.org/10.1016/j.immuni.2021.12.015.

32. Chen, X., Zheng, Y.H., Liu, S.M., Yu, W.J., and Liu, Z.D. (2022). CD169 subcapsular sinus macrophage-derived microvesicles are associated with light zone follicular dendritic cells. Eur. J. Immunol. *52*, 1581–1594. https://doi.org/10.1002/eji.202249879.

33. Song, W., and Craft, J. (2019). T follicular helper cell heterogeneity: Time, space, and function. Immunol. Rev. *288*, 85–96. https://doi.org/10.1111/imr.12740.

34. Crotty, S. (2019). T Follicular Helper Cell Biology: A Decade of Discovery and Diseases. Immunity *50*, 1132–1148. https://doi.org/10.1016/j.immuni.2019.04.011.

35. Gelfand, E.W. (2017). Importance of the leukotriene B4-BLT1 and LTB4-BLT2 pathways in asthma. Semin. Immunol. *33*, 44–51. https://doi.org/10.1016/j.smim.2017.08.005.

36. He, R., Chen, Y., and Cai, Q. (2020). The role of the LTB4-BLT1 axis in health and disease. Pharmacol. Res. *158*, 104857.

37. Miyahara, N., Ohnishi, H., Miyahara, S., Takeda, K., Matsubara, S., Matsuda, H., Okamoto, M., Loader, J.E., Joetham, A., Tanimoto, M., et al. (2009). Leukotriene B4 Release from Mast Cells in IgE-Mediated Airway Hyperresponsiveness and Inflammation. Am. J. Respir. Cell Mol. Biol. *40*, 672–682. https://doi.org/10.1165/rcmb.2008-0095OC.

38. Terawaki, K., Yokomizo, T., Nagase, T., Toda, A., Taniguchi, M., Hashizume, K., Yagi, T., and Shimizu, T. (2005). Absence of Leukotriene B4 Receptor 1 Confers Resistance to Airway Hyperresponsiveness and Th2-Type Immune Responses. J. Immunol. *175*, 4217–4225. https://doi.org/10.4049/jimmunol.175.7.4217.

39. Miyahara, N., Takeda, K., Miyahara, S., Matsubara, S., Koya, T., Joetham, A., Krishnan, E., Dakhama, A., Haribabu, B., and Gelfand, E.W. (2005). Requirement for Leukotriene B4Receptor 1 in Allergen-induced Airway Hyperresponsiveness. Am. J. Respir. Crit. Care Med. *172*, 161–167. https://doi.org/10.1164/rccm.200502-205OC.

40. Hartenstein, B., Teurich, S., Hess, J., Schenkel, J., Schorpp-Kistner, M., and Angel, P. (2002). Th2 cell-specific cytokine expression and allergen-induced airway inflammation depend on JunB. Embo J *21*, 6321–6329. https://doi.org/10.1093/emboj/cdf648.

41. Li, B., Tournier, C., Davis, R.J., and Flavell, R.A. (1999). Regulation of IL-4 expression by the transcription factor JunB during T helper cell differentiation. Embo J *18*, 420–432. https://doi.org/10.1093/emboj/18.2.420.

42. Gaudreault, E., and Gosselin, J. (2009). Leukotriene B4 Potentiates CpG Signaling for Enhanced Cytokine Secretion by Human Leukocytes. J. Immunol. *183*, 2650–2658. https://doi.org/10.4049/jimmunol.0804135.

43. Li, P., Oh, D.Y., Bandyopadhyay, G., Lagakos, W.S., Talukdar, S., Osborn, O., Johnson, A., Chung, H., Maris, M., Ofrecio, J.M., et al. (2015). LTB4 promotes insulin resistance in obese mice by acting on macrophages, hepatocytes and myocytes. Nat. Med. *21*, 239–247. https://doi.org/10.1038/nm.3800.

44. Koizumi, S.-i., Sasaki, D., Hsieh, T.-H., Taira, N., Arakaki, N., Yamasaki, S., Wang, K., Sarkar, S., Shirahata, H., Miyagi, M., and Ishikawa, H. (2018). JunB regulates homeostasis and suppressive functions of effector regulatory T cells. Nat. Commun. *9*, 5344. https://doi.org/10.1038/s41467-018-07735-4.

45. Tager, A.M., Bromley, S.K., Medoff, B.D., Islam, S.A., Bercury, S.D., Friedrich, E.B., Carafone, A.D., Gerszten, R.E., and Luster, A.D. (2003). Leukotriene B4 receptor BLT1 mediates early effector T cell recruitment. Nat. Immunol. *4*, 982–990. https://doi.org/10.1038/ni970.

46. Nelson, C.S., Podestà, M.A., Gempler, M.G., Lee, J.-M., Batty, C.J., Mathenge, P.G., Sainju, A., Chang, M.R., Ke, H., Chandrakar, P., et al. (2025). The inflammaging microenvironment induces dysfunctional rewiring of Tfh cell differentiation. JCI Insight *10*, e187271. https://doi.org/10.1172/jci.insight.187271.

STAR★METHODS

KEY RESOURCES TABLE

REAGENT or RESOURCE	SOURCE	IDENTIFIER
Antibodies		
anti- CD45R/B220	BD Biosciences	Cat# 552771, RRID:AB_394457
anti- CD45R/B220	BioLegend	Cat# 103241, RRID:AB_11204069
anti- CD19	BD Biosciences	Cat# 551001, RRID:AB_394004
anti- GL7 (T and B cell Activation Marker)	BioLegend	Cat# 144606, RRID:AB_2562185
anti- CD38	BioLegend	Cat# 102727, RRID:AB_2616967
anti- CD95	BD Biosciences	Cat# 557653, RRID:AB_396768
anti- IgG1	BD Biosciences	Cat# 562107, RRID:AB_10894002
anti- IgE	BioLegend	Cat# 406905, RRID:AB_493288
anti- IgE	BioLegend	Cat# 406907, RRID:AB_493291
anti- CD4	BioLegend	Cat# 100414, RRID:AB_312699
anti- CD4	BioLegend	Cat# 100434, RRID:AB_893324
anti- CD44	BioLegend	Cat# 103044, RRID:AB_2650923
anti- CD45	BioLegend	Cat# 103151, RRID:AB_2565884
anti- CD8a	BioLegend	Cat# 100733, RRID:AB_2075239
anti- CD11b	BioLegend	Cat# 101227, RRID:AB_893233
anti- CD11b	Thermo Fisher Scientific	Cat# 17-0112-81, RRID:AB_469342
anti- CD11c	BioLegend	Cat# 117327, RRID:AB_2129642
anti- TER-119	BioLegend	Cat# 116227, RRID:AB_893638
anti- F4/80	BioLegend	Cat# 123127, RRID:AB_893496
anti- MHCII(I-A/I-E)	BioLegend	Cat# 107625, RRID:AB_2191072
anti- Ly-6G	BioLegend	Cat# 127639, RRID:AB_2565880
anti- Ly-6G/Ly-6c(Gr1)	BioLegend	Cat# 108427, RRID:AB_893561
anti- CD170 (Siglec-F)	BioLegend	Cat# 155505, RRID:AB_2750234
anti- CD279 (PD-1)	Thermo Fisher Scientific	Cat# 11-9985-85, RRID:AB_465473
anti- CXCR5	BD Biosciences	Cat# 551960, RRID:AB_394301
anti- IL13	Thermo Fisher Scientific	Cat# 25-7133-80, RRID:AB_2573529
anti- IL4	BioLegend	Cat# 504119, RRID:AB_10896945
anti- IL4	BioLegend	Cat# 504105, RRID:AB_315319
anti- IL5	BioLegend	Cat# 504305, RRID:AB_315329
anti- CXCR6	Biolegend	Cat# 151103, RRID: AB_2566545
anti- CXCR5	BD Biosciences	Cat# 552118, RRID: AB_394337
anti- CD279(PD-1)	Thermo Fisher Scientific	Cat# 25-2799-42, RRID: AB_10853804
anti- CD19	Biolegend	Cat# 302230, RRID: AB_2073119
anti- CD4	Thermo Fisher Scientific	Cat# 11-0049-42, RRID: AB_1659694
CD3e Functional Grade Monoclonal Antibody (145-2C11)	Thermo Fisher Scientific	Cat# 16-0031-85, RRID:AB_468848
CD28 Functional Grade Monoclonal Antibody (37.51)	Thermo Fisher Scientific	Cat# 16-0281-85, RRID:AB_468922
anti-mouse IFN-g	Bioxcell	Cat#: BE0055, RRID:AB_1107694
anti-mouse IL-4	Bioxcell	Cat#: BE0045, RRID: AB_1107707

(*Continued on next page*)

Continued

REAGENT or RESOURCE	SOURCE	IDENTIFIER
Goat Anti-Mouse IgE-AP	Southern Biotech	Cat# 1110-04, RRID:AB_2794603
Goat Anti-Mouse IgG1, Human ads-AP	Southern Biotech	Cat# 1070-04, RRID:AB_2794411
Chemicals, peptides, and recombinant proteins		
PE streptavidin	Biolegend	Cat# 405203
CP-105696	MCE	Cat# 158081-99-3
NP-4-BSA	Biosearch	Cat# *N*-5050L
NP-16-BSA	Biosearch	Cat# *N*-5050H
House dust mite extract	Greer	Lot# 248041
Collagenase IV	Sigma-Aldrich	Cat# C5138-1g
Deoxyribonuclease I	Transgen	Cat# GE101-01
LIVE/DEAD Fixable Violet Dead Cell Stain Kit	Thermo Fisher Scientific	Cat# L34964
eBioscience™ Cell Stimulation Cocktail (plus protein transport inhibitors)	Thermo Fisher Scientific	Cat# 00-4975-93
Protease Inhibitor	Selleck	Cat# B14001
Percoll	Cytiva	Cat# 17089101
Pierce™ Diethanolamine Substrate Buffer (5X)	Thermo Fisher Scientific	Cat# 34064
TRIzol	Invitrogen	Cat# 15596018
Leukotriene B4	MCE	Cat# 71160-24-2
T-5224	Selleck	Cat# S8966
JNK Inhibitor IX	Selleck	Cat# 312917-14-9
Murine RNase Inhibitor	Vazyme	Cat# DD4102
PMA	Sigma-Aldrich	Cat# P1585-1MG
Ionomycin	Enzo Life Sciences	Cat# ALX-450-007-M001
Brefeldin A	BioLegend	Cat# 420601
Recombinant human IL2	Peprotech	Cat# AF-200-02-100
Recombinant mouse IL2	R&D	Cat# 402-ML-020
Recombinant mouse IL6	Bioxcell	Cat# BE0046
Recombinant mouse IL21	novoprotein	Cat# CK10
NP(16)-OVA (Ovalbumin)	Biosearch Technologies	Cat# *N*-5051
LPS(055:B5)	Sigma	Cat# L2880
HDM	Greer Labs	Cat#NC9756554
Critical commercial assays		
eBioscience™ Intracellular Fixation & Permeabilization Buffer Set	ThermoFisher Scientific	Cat# 88-8824-00
EasySep™ Mouse $CD4^+$ T cell Isolation Kit	STEMCELL Technologies	Cat# 19852
EasySep™ Mouse Naive $CD4^+$ T cell Isolation Kit	STEMCELL Technologies	Cat# 19765
SBA Clonotyping System-AP	SouthernBiotech	Cat# 5300-04
LTB4(Leukotriene B4) ELISA Kit	Sangon Biotech	Cat# D751028-0096
Mouse IL-13 enzyme-linked immunoassay kit	HUABIO	Cat# EM0007
Dynabeads™ Human T-Activator CD3/CD28	ThermoFisher Scientific	Cat# 11161D
ProteanFect™ Max Mouse Immunocyte Transfection Kit	NanoportalBiotech	Cat# PT03
ProteanFect™ CRISPRMax Transfection Kit	NanoportalBiotech	Cat# PT05
ChIP-IT Express Enzymatic Shearing Kit	Active Motif	Cat# 53035
PrimeScript™ RT reagent Kit	Takara	Cat# RR420A

(*Continued on next page*)

Continued

REAGENT or RESOURCE	SOURCE	IDENTIFIER
2×Universal Blue SYBR Green qPCR Master Mix	Servicebio	Cat# G3326-01
Deposited data		
Raw and analyzed data	This study	CRA028468
Raw and analyzed data	Yeh CH et al.[31]	GSE147035
Raw and analyzed data	Gowthaman U et al.[12]	GSE132798
Raw and analyzed data	Kuwahara M et al.[25]	GSE65084
Experimental models: Organisms/strains		
Mouse: Bach2$^{fl/fl}$	Zhang et al.[22]	N/A
Mouse: Ltb4r1$^{fl/fl}$	This study	N/A
Mouse: C57BL/6: C57BL/6J	The Jackson Laboratory	RRID:IMSR_JAX:000664
Mouse: B6.Cg-Tg(Cd4-cre)1Cwi/BfluJ	The Jackson Laboratory	RRID:IMSR_JAX:022071
Mouse: Foxp3YFP-Cre: B6.129(Cg) Foxp3tm4(YFP/icre)Ayr/J	The Jackson Laboratory	RRID:IMSR_JAX:016959
Oligonucleotides		
mIl4 QPCR primer: F: 5′-AGATCATCGGCATTTTGAACG-3′ R: 5′-TTTGGCACATCCATCTCCG-3	Gowthaman U et al.[12]	N/A
mIl13 QPCR primer: F: 5′-GCTTATTGAGGAGCTGAGCAACA-3′ R: 5′-GGCCAGGTCCACACTCCATA-3′	Gowthaman U et al.[12]	N/A
mIl5 QPCR primer: F: 5′- TGGAGATTCCCATGAGCAC-3′ R: 5′- AGGGACAGGAAGCCTCATC-3′	This paper	N/A
mCxcr5 QPCR primer: F: 5′- *ATGAACTACCCACTAACCCTGG*-3′ F: 5′- *TGTAGGGGAATCTCCGTGCT*-3′	This paper	N/A
m Pdcd1 QPCR primer: F: 5′- ACCCTGGTCATTCACTTGGG-3′ F: 5′- CATTTGCTCCCTCTGACACTG-3′	This paper	N/A
mGata3 QPCR primer: F: 5′- GAAGGCATCCAGACCCGAAAC -3′ F: 5′- ACCCATGGCGGTGACCATGC-3′	This paper	N/A
mBLT1 QPCR primer: F: 5′- ATGGCTGCAAACACTACATCTC -3′ F: 5′- GACCGTGCGTTTCTGCATC-3′	This paper	N/A
mJunB QPCR primer: F: 5′- GACCTGCACAAGATGAACCACG -3′ F: 5′- ACTGCTGAGGTTGGTGTAGACG-3′	This paper	N/A
mActb QPCR primer: F: 5′- TCCGGCACTACCGAGTTATC-3′ F: 5′- GATCCGGTGTAGCAGATCGC-3′	This paper	N/A
hIL4 QPCR primer: F: 5′- CCAGGCAGCGAGTGTCC-3′ R: 5′- CACCGAGTTGACCGTAACAGAC-3′	This paper	N/A
hIL13 QPCR primer: F: 5′- CCTCATGGCGCTTTTGTTGAC-3′ R: 5′- TCTGGTTCTGGGTGATGTTGA-3′	This paper	N/A
hIL5 QPCR primer: F: 5′- GGAATAGGCACACTGGAGAGTC-3′ R: 5′- CTCTCCGTCTTTCTTCTCCACAC-3′	This paper	N/A
hBLT QPCR primer: F: 5′- CCTGTGTCACTATGTCTGCGGA-3′ R: 5′- ATCGCCTTGGTGCGTAGCTTCT-3′	This paper	N/A

(*Continued on next page*)

Continued

REAGENT or RESOURCE	SOURCE	IDENTIFIER
hBACH2 QPCR primer: F: 5′- CTGCCGCAAAAGGAAACTGGAC-3′ R: 5′- GGAAAGGCAGGAGAAGTTGTCC-3′	This paper	N/A
hGAPDH QPCR primer: F: 5′- GAGTCCACTGGCGTCTTCAC-3′ R: 5′- ATCTTGAGGCTGTTGTCATACTTCT-3′	This paper	N/A
JunB#1 ChIP-QPCR primer: F: 5′- TGGGACGACAGTGAGTCTGA-3′ R: 5′- CTTCCTGGCCAGAGAGTTTG-3′	Kuwahara M et al.[25]	N/A
JunB#2 ChIP-QPCR primer: F: 5′- ATGCCTGCCCTAGCTACCTC-3′ R: 5′- CTTGCCTTCCTACCACTGGA-3′	Kuwahara M et al.[25]	N/A
Bach2 ChIP-QPCR primer: F: 5′- GCTTCGTGGTCAAGCTACTG-3′ R: 5′- AAGTCATGAAGCTGTCGGTGG-3′	This paper	N/A
mJunb#1 siRNA: F: 5′- GCAUCAAAGUGGAGCGAAATT-3′ R: 5′- UUUCGCUCCACUUUGAUGCTT-3′	This paper	N/A
mJunb#2 siRNA: F: 5′- GCCUGUCUACACGACUATT-3′ R: 5′- UAGUCGUGUAGAGACAGGCTT-3′	This paper	N/A
mJunb#3 siRNA: F: 5′- GGAGGACAAGGUGAAGACATT-3′ R: 5′- UGUCUUCACCUUGUCCUCCTT-3′	This paper	N/A
hBACH2#1 siRNA: F: 5′- CGCUGGUUGGACAGACAAATT-3′ R: 5′- UUUGUCUGUCCAACCAGCGTT-3′	This paper	N/A
hBACH2#2 siRNA: F: 5′- GUACCAAGAAUGUCUAUAATT-3′ R: 5′- UUAUAGACAUUCUUGGUACTT-3′	This paper	N/A
hBACH2#3 siRNA: F: 5′- GGGUGAGCAUUUGGACAATT-3′ R: 5′- UUGUCCAAACUGCUCACCCTT-3′	This paper	N/A
Negtive Control siRNA: F: 5′- UUCUCCGAACGUGUCACGUTT-3′ R: 5′- ACGUGACACGUUCGGAGAATT -3′	This paper	N/A
Software and algorithms		
FlowJo	Tree Star	https://www.flowjo.com/solutions/flowjo/downloads
GraphPad Prism	GraphPad	https://www.graphpad.com/
GSEA	–	http://software.broadinstitute.org/gsea/index.jsp
ImageJ	National Institutes of Health	https://imagej.nih.gov/ij

EXPERIMENTAL MODEL AND STUDY PARTICIPANT DETAILS

Mouse models

All mice were crossed on C57BL/6 background. *Bach2*$^{fl/fl}$ mice have been described previously.[22] *Ltb4r1*$^{fl/fl}$ mice were generated at the Cyagen Biosciences (floxed exon 2). *Cd4-Cre* and *Foxp3-Cre* transgenic mice were purchased from The Jackson Laboratory. All mice were housed in specific pathogen-free facilities. All animal experiments were reviewed and approved by the Institutional Animal Care and Use Committee (IACUC) of Shanghai Jiao Tong University, School of Medicine (Protocol JUMC2023-103-A). Unless otherwise stated, 6-to 8-week old mice with both sexes were used.

METHOD DETAILS

Immunization

For the NP16-OVA induced asthma model, mice were immunized intranasally (i.n) with 2 μg of LPS (Sigma) and 25μg of NP16-OVA (LGC Biosearch Technologies) for primary immunizations. Mice were boosted twice (i.n) with 10 μg of NP16-OVA on day 12 and day 19 after primary immunization. 7 days after the last administration, mice were sacrificed, and organs were dissected for analysis. For the HDM-induced asthma model, mice were immunized (i.n) with 25 μg of HDM (Greer Labs) and 25μg of NP16-OVA (LGC Biosearch Technologies) for 4 consecutive days starting on day 1, considered as the sensitization stage. Then, on day 15, mice were challenged (i.n.) with 12.5 μg of HDM daily for 4 days. On day 20, mice were sacrificed, and organs were dissected for analysis and analyzed.

Flow cytometry and cell sorting

Bronchoalveolar lavage fluid (BALF) was collected by two consecutive flushes of the lung with 1 mL PBS. Blood was taken to screen for serum antibodies. Lungs were isolated, cut into small fragments and digested for 45 min at 37 °Cwith 0.6 mg/mL collagenase A (Sigma) and 30 mg/mL DNase I (Sigma) in RPMI-1640 medium (GIBCO) containing 2% fetal bovine serum. Digested lungs were mechanically disrupted by passage through 70 μm cell strainers. The cell pellets were re-suspended in 30% Percoll, carefully layered onto 70% Percoll and centrifuged at 800 g at RT for 20 min (ascending rate: 5; descending rate: 1). The cells at the interface between 30% and 70% Percoll were collected and washed twice in cold PBS. Spleens were homogenized by filtering through 70 μm cell strainers and red blood cells were lysed with ACK buffer. Lung draining mediastinal lymph nodes were homogenized by filtering through 70 μm cell strainers. Single-cell suspensions of tissues above were prepared from fresh tissues and Fc receptors were blocked with anti-mouse CD16/32 (BD-Biosciences), followed by surface-stained in FACS buffer with monoclonal antibodies. For intracellular cytokine staining, cells were first stimulated with PMA (50 ng/mL, Sigma-Aldrich) and ionomycin (500 ng/mL, Sigma-Aldrich) for 4 h, and brefeldin A (2 μg/mL, Sigma-Aldrich) was added for the last 2 h. After surface staining, cells were fixed and permeabilized with

eBioscience Intracellular Fixation & Permeabilization Buffer Set. After staining, data were collected with the LSRFortessa X-20 (BD) and analyzed with FlowJo software (Tree Star). The information of antibodies for Flow cytometry analysis is provided in key resources table.

In vivo treatment of Ltb4r1 inhibitor

To inhibit Ltb4r1 signaling, mice were immunized as previously described and subsequently administered either the selective Ltb4r1 antagonist CP-105696 (100 mg/kg) or vehicle control (10% DMSO, 40% PEG300, 5% Tween-80, 45% saline) via intragastric gavage at specified time points (days 11, 12, 18, 19, 20, 23, and 25 post immunizations).

In vitro Tfh-like cell differentiation and inhibitor treatment

$CD4^+$ T cells were enriched from the spleens and peripheral lymph nodes by mouse $CD4^+$ T cell isolation kit (STEMCELL Technologies). Sorted $CD4^+$ T cells were suspended in RPMI 1640 medium (GIBCO) supplemented with 100 U/mL penicillin, 100 μg/mL streptomycin, 0.05 mM β-mercaptoethanol and 10% fetal bovin serum (GIBCO). Cells were activated with plate-bound anti-mouse CD3ε (5 μg/mL, BioLegend) and anti-mouse CD28 (5 μg/mL; BioLegend) for 48 h. Then, these cells were washed and transferred to a new plate and further expanded in medium with 20 ng/mL IL-6, 20 ng/mL IL-21 (both from PeproTech), 10 μg/mL anti-IFN-g and 10 μg/mL anti-IL-4 (both from BioLegend) for 4 days to induce T follicular helper cell-like cells. On the final day of culture, cells were treated with either 0.1 μM LTB4 (MedChemExpress), 50 μM T-5224 (Selleckchem), 10 μM JNK Inhibitor (Selleckchem), or an equivalent volume of DMSO as a vehicle control.

siRNA knockdown and inhibitor treatment in Tfh cells cultured *in vitro*

Total Tfh cells were isolated from WT or T-*Bach2*$^{-/-}$ mice and activated with plate-bound anti-mouse CD3ε (5 μg/mL) and anti-mouse CD28 (5 μg/mL; both from BioLegend) for 48 h. For siRNA-mediated gene silencing, cells were transfected using the ProteanFect Max Mouse Immunocyte Transfection Kit (Nanoportal Biotech) according to the manufacturer's protocol, with co-transfection of mEGFP as a transfection efficiency marker. Two days after transfection, cells were treated with either 0.1 μM LTB4 (MedChemExpress), 50 μM T-5224 (Selleckchem), 10 μM JNK Inhibitor (Selleckchem), or an equivalent volume of DMSO.

Human $CD4^+CXCR5^+PD1^+$ Tfh cells were sorted from tonsils using FACSAria III cell sorter (BD Biosciences) at the Shanghai Institute of Immunology Core Facility. These cells were further activated using Dynabeads Human T-Activator CD3/CD28 (Thermo Fisher scientific) and 30 U/mL rIL-2 for 48 h. For siRNA-mediated gene silencing, cells were transfected using the ProteanFect CRISPRMax Gene Editing Transfection Kit (Nanoportal Biotech) according to the manufacturer's protocol, with co-transfection of mEGFP as a transfection efficiency marker. Subsequently, transfected cells were cultured in complete T cell culture medium for 24 h, consisting of RPMI 1640 medium supplemented with 100 U/mL of penicillin, 100 μg/mL of streptomycin, 0.05 mM of β-mercaptoethanol, 10% fetal bovin serum (GIBCO) and 30 U/mL rIL-2 (PeproTech). These cells were further treated with either 0.1 μM LTB4 (MedChemExpress) or an equivalent volume of DMSO vehicle control for 24 h. Mouse and human GFP^+ cells were sorted using a FACSAria III cell sorter (BD Biosciences) for analysis. The sequences of siRNA are listed in key resources table.

Quantitative PCR (QPCR)

RNA was extracted using TRIzol (Invitrogen) following the manufacturer's protocol, and reverse-transcribed with PrimeScript RT reagent Kit (Takara). QPCR was carried out with TB Green Premix Ex TaqTM (Takara). All quantitative data of mouse samples were normalized to the amount of *Actb*. All quantitative data of human sample were normalized to the amount of *GAPDH*. Gene-specific primers are listed in key resources table.

In vitro Tfh-like cell differentiation

$CD4^+$ T cells were enriched from the spleens and peripheral lymph nodes by mouse $CD4^+$ T cell isolation kit (STEMCELL Technologies). Sorted $CD4^+$ T cells were suspended in RPMI 1640 medium (GIBCO) supplemented with 100 U/mL penicillin, 100 μg/mL streptomycin, 0.05 mM β-mercaptoethanol and 10% fetal bovin serum (GIBCO). Cells were activated with plate-bound anti-mouse CD3ε (5 μg/mL, BioLegend) and anti-mouse CD28 (5 μg/mL; BioLegend) for 48 h. Then, these cells were washed and transferred to a new plate and further expanded in medium with 20 ng/mL IL-6, 20 ng/mL IL-21 (both from PeproTech), 10 μg/mL anti-IFN-g and 10 μg/mL anti-IL-4 (both from BioLegend) for 4 days to induce T follicular helper cell-like cells.

Chromatin immunoprecipitation (ChIP)-QPCR analysis

Chromatin was cross-linked with 1% formaldehyde (Sigma-Aldrich) for 10 min at room temperature, followed by quenching with 0.125 M glycine. Cells were lysed, and chromatin was sheared by sonication to generate DNA fragments of 300–500 bp. Immunoprecipitation was performed overnight at 4°C using either anti-BACH2 antibodies, anti-JunB antibodies (Cell Signaling Technology) or anti-IgG antibodies (Cell Signaling Technology) as a negative control. Following extensive washing, immunocomplexes were eluted in ChIP elution buffer and cross-links were reversed by incubation at 65°C overnight. Purified DNA was analyzed by QPCR using the primers listed in key resources table.

Enzyme-linked immunosorbent assay (ELISA)

To measure NP-specific and total IgE in serum and BALF, IgG were depleted by incubating with protein G-Sepharose (GE Healthcare) overnight at 4°C. To measure NP-specific antibodies, the plates were coated with 20 μg/mL NP4-BSA or NP26-BSA (Bioresearch) in carbonate buffer at 4°C overnight. To detect total IgE in serum and BALF, the plates were coated overnight with 2 μg/mL anti-mouse IgE captured antibodies (BD Pharmingen). After coating, plates were blocked with 1% BSA in PBS at 37°C for 1 h. Subsequently, serially diluted serum samples (1:300 for IgG1, 1:30 for IgE) or BALF samples (1:10 for IgG1, undiluted for IgE) were added and incubated at 37°C for 1 h. NP-specific and total antibodies of each isotype were detected using anti-IgE-AP or anti-IgG1-AP antibodies (Southern Biotech), followed by incubation at 37°C. A substrate solution was prepared using diethanolamine substrate buffer (Thermo Scientific) and *p*-nitrophenyl phosphate (Thermo Scientific). Each well was filled with 100 μL of substrate solution, and color development was measured at 405 nm using a microplate reader (BioTek Synergy HT). LTB4 levels were measured using a commercial kit (Sangon) according to the manufacturer's protocol. IL-13 concentrations in the supernatants of Tfh cells stimulated *in vitro* with anti-CD3 and anti-CD28 antibodies for 2 days were quantified using a commercial kit (HUABIO) according to the manufacturer's instructions.

Histological analysis

Lungs were removed from mice after lavage with PBS and then fixed with 4% paraformaldehyde. Lobes were sectioned sagitally, embedded in paraffin, cut into 5-μm sections, and stained with hematoxylin and eosin for analysis. An inflammation score was assigned in a blinded fashion. The score of peribronchiolar and perivascular inflammation was determined as follows: 0, normal; 1, few cells; 2, a ring of inflammatory cells one cell layer deep; 3, a ring of inflammatory cells two to four cells deep; and 4, a ring of inflammatory cells of more than four cells deep. Additional sections were stained with Alcian blue-periodic acid schiff (AB-PAS) for analysis of mucus-containing cells. Scoring was performed by examining at least 20 consecutive fields. Numerical scores for the abundance of AB-PAS-positive goblet cells in each airway were determined as follows: 0, <5% goblet cells; 1, 5–25%; 2, 25–50%; 3, 50–75%; and 4, >75%, with 0 being negative and 1–4 being positive for AB-PAS-staining bronchi.

Immunofluorescence

To examine distribution patterns of $Cxcr6^+$ cells, medLNs collected from immunized wild-type mice on day 27 were fixed in 4% paraformaldehyde for 4 hour at 4°C. After fixation, tissues were washed three times with PBS and left overnight in a 30% sucrose solution at 4°C. Tissues were embedded in Tissue-Tek O.C.T. compound and were sliced in sections of 14 mm using a cryostat (Leica). Sections were blocked for 1 h using 10% sheep serum and 0.3% Triton X-100 and stained with PE anti-mouse T and B cell activation antigen (1:200), APC anti-mouse CD4 (1:500), PE anti-mouse IgD (1:500), and primary unlabeled antibodies to CXCR6 (1:200) overnight. After washing, slides were stained with Goat anti-Rabbit IgG (H + L) Cross-Adsorbed Secondary Antibody Alexa Fluo-488 (1:200) and DAPI for 1 h at room temperature. After mounting, images were captured using Leica SP8 confocal microscope with a ×40 oil immersion objective, Olympus SLIDEVIEW VS200 with a ×20 dry immersion objective and processed with Fiji (version 2.9.0).

For sorted $CD4^+$ T cells immunofluorescence analyses, $CD4^+$ T cells were centrifuged at 300 rpm into the Poly-L-Lysine Solution treated slides in 24-well plates, fixed with paraformaldehyde and permeabilized with 0.2% Triton X-100 in PBS, then blocked

following stained with APC anti-mouse CD4 (1:500) and primary unlabeled antibodies to JunB Rabbit mAb (1:200). After washing, slides were stained with Goat anti-Rabbit IgG (H + L) Cross-Adsorbed Secondary Antibody FITC (1:200) and DAPI. Images were acquired on Leica Sp8 confocal microscope with a ×40 oil immersion objective. The information of antibodies for immunofluorescence is provided in KEY RESOURCES TABLE.

Single-cell RNA-sequencing (scRNA-seq) and data analysis

Total B220^{-}CD4^{+}CD44^{+}CXCR5^{+}PD-1^{+} Tfh cells were isolated from the medLNs of 6-8-week-old T-*Bach2*$^{-/-}$ and WT mice following LPS+OVA immunization. Approximately 12,000 Tfh cells (pooled equally from three mice per genotype) were loaded into one channel of Single Cell Chip A using a Chromium Single Cell 5′ Reagent Kit (V3) (10x Genomics) to prepare scRNA-seq libraries to prepare scRNA-seq libraries following the manufacturer's protocols. Libraries were sequenced on an Illumina NovaSeq6000 sequencer. The raw fastq files were processed using the 10X Genomics Cell Ranger pipeline (version 6.0.1, 10X Genomics, mm10 genome as reference) and Seurat (v4.1.1) R package. Quality control filtering was performed by removing low-quality cells or doublets with less than 200 or more than 6000 detected genes, and cells with the percentage of reads mapped to mitochondrial genes exceeding 10%. The gene expression matrix of scRNA-seq was normalized and scaled using Seurat NormalizeData and ScaleData functions. UMAP embedding was used for two-dimensional visualization. FindNeighbors and FindClusters functions were used for the unsupervised clustering. In this dataset, six Tfh cell clusters were annotated on the basis of published canonical marker genes.[10,46] To define the transcriptional features of Alternaria extract–induced Tfh13 cells, we reanalysed a publicly available scRNA-seq dataset (GSE132798) using the same analytical pipeline. This dataset was generated from sorted total CXCR5^{+}PD-1^{+} Tfh cells and was therefore expected to comprise cellular states comparable to those identified in our dataset. Accordingly, we performed a guided clustering to assign these cells into six Tfh cell clusters based on the canonical marker genes defined in analysis of our dataset. The inferred developmental trajectory of Tfh-lineage cells was analyzed using Monocle 3.

Differentially expressed genes (DEGs) were identified using the Wilcoxon rank-sum test implemented in the FindMarkers function of the Seurat package. For group-level comparison, cells of interest were analyzed between T-*Bach2*$^{-/-}$ and WT T cell populations. DEGs with adjusted p-values <0.05 and the highest absolute log2 fold changes were retained for downstream analysis. Volcano plots visualizing DEGs were generated using the volcano R package.

To assess functional alterations across T cell subsets, gene set variation analysis (GSVA) was performed. KEGG pathway enrichment analysis was conducted to interpret the biological significance of DEGs. DEGs were annotated to KEGG pathways, and significantly enriched pathways were defined by adjusted p-values <0.05. The top 10 most significantly enriched pathways were visualized to highlight key immune-related signaling cascades.

In addition, Gene Set Enrichment Analysis (GSEA) was performed using the clusterProfiler R package to identify pathway-level shifts based on ranked gene expression. Genes were ranked by log2 fold change and used as input for the GSEA function. Pathways with nominal p-values <0.05 were considered significantly enriched. Enrichment plots were generated using the gseaplot2 function.

scTCR-seq

The TCR sequence data were processed with the CellRanger VDJ pipeline. After V(D)J sequence assembly and clonotype calling, the outputs were integrated with gene expression data according to the same barcodes, and only cells detected with single paired TCRs (α and β chains) were reserved for further analysis. T cells with identical α-β CDR3 pairs were recognized as the same clonotype. Expanded clone types were identified based on the presence of two or more T cells expressing the same paired TCR α and TCRβ chains. Clonal overlap between T cell compartments was visualized using circlize v.0.4.15.

QUANTIFICATION AND STATISTICAL ANALYSIS

The number of mice per group, number of replicates and the nature of error bars are indicated in the legend of each figure. Center bars indicate mean unless otherwise specified. Statistical significance was determined with Graphpad Prism Version 7.0 using the tests indicated in each figure legend. p value <0.05 is considered statistically significant, and the level of significance was indicated as $^{*}p < 0.05$ and $^{**}p < 0.01$. p-values >0.05 are considered to be not significant (ns).